Inorganic Chemistry
Article

Inorg. Chem. **2009**, *48*, 11161–11175 **11161**
DOI: 10.1021/ic901637b

Controlling Electron Transfer through the Manipulation of Structure and Ligand-Based Torsional Motions: A Computational Exploration of Ruthenium Donor−Acceptor Systems using Density Functional Theory

Heather A. Meylemans and Niels H. Damrauer*

Department of Chemistry and Biochemistry, University of Colorado, Boulder, Colorado 80309

Received August 14, 2009

Computational studies using density functional theory (DFT) are reported for a series of donor−acceptor (DA) transition metal complexes and related excited-state and electron transfer (ET) photoproduct models. Three hybrid Hartree−Fock/DFT (HF/DFT) functionals, B3LYP, B3PW91, and PBE1PBE, are employed to characterize structural features implicated in the dynamical control of productive forward and energy wasting back ET events. Energies and optimized geometries are reported for the lowest energy singlet state in $[Ru(dmb)_2(bpy\text{-}\phi\text{-}MV)]^{4+}$ (**DA1**), $[Ru(dmb)_2(bpy\text{-}o\text{-}tolyl\text{-}MV)]^{4+}$ (**DA2**), $[Ru(dmb)_2(bpy\text{-}2,6\text{-}Me_2\text{-}\phi\text{-}MV)]^{4+}$ (**DA3**), and $[Ru(tmb)_2(bpy\text{-}2,6\text{-}Me_2\text{-}\phi\text{-}MV)]^{4+}$ (**DA3′**), where dmb is 4,4′-dimethyl-2,2′-bipyridine, tmb is 4,4′,5,5′-tetramethyl-2,2′-bipyridine, MV is methyl viologen, and ϕ is a phenylene spacer. These indicate that the dihedral angle θ_1 between the aryl substituent and the bipyridine fragment to which it is bound, systematically increases with the addition of steric bulk. Energies, optimized geometries, and unpaired electron spin densities are also reported for the lowest energy triplet state of $[Ru(dmb)_2(4\text{-}p\text{-}tolyl\text{-}2,2'\text{-}bipyridine)]^{2+}$ (**D1***), $[Ru(dmb)_2(4\text{-}(2,6\text{-}dimethylphenyl)\text{-}2,2'\text{-}bipyridine)]^{2+}$ (**D2***), $[Ru(dmb)_2(4\text{-}mesityl\text{-}2,2'\text{-}bipyridine)]^{2+}$ (**D3***), and $[Ru(tmb)_2(4\text{-}mesityl\text{-}2,2'\text{-}bipyridine)]^{2+}$ (**D3′***). Each of these serves as a model of a reactant excited state in the forward electron-transfer photochemistry allowing us to qualify and quantify the role of excited-state intraligand electron delocalization in driving substantial geometry changes (especially with respect to θ_1) relative to its respective **DA** counterpart. Next, energies, optimized geometries, and spin densities are reported for the lowest energy triplet of each **DA** species: ^{3}**DA1**, ^{3}**DA2**, ^{3}**DA3**, and ^{3}**DA3′**. These are used to model the ET photoproduct and they indicate that θ_1 increases following ET, thus, verifying switch-like properties. Finally, we report data for geometry optimized **DA1** and ^{3}**DA1** in a continuum model of room temperature acetonitrile. This study shows a complete recovery of θ_1 to its ground state value which has implications in efforts to trap electrons in charge-separated states.

Introduction

The control of structural and electronic properties in visible chromophoric molecules and materials is a critical research direction in efforts to achieve efficient conversion of solar photons to electrical potential or storable fuels.[1−5] One central issue involves achieving light-driven charge separation, that is, the production of redox equivalents, at complex interfaces. This is true in systems ranging from heterojunction solar cell materials, both inorganic[4,6,7] and organic,[8−11] to Donor−Acceptor (DA) assemblies being designed and explored for solar fuels formation.[3,5,12−14] In the interest of achieving fast forward/productive electron transfer (ET) events under conditions of small interfacial electronic coupling, researchers (and natural systems) tend to rely on large negative reaction free energies. The downside to this is inefficiency in the total conversion of a photon's energy to electrical or chemical potential. One might consider systems with larger interfacial electronic coupling; however, energy

*To whom correspondence should be addressed. E-mail: niels.damrauer@colorado.edu.

(1) *Basic Research Needs for Solar Energy Utilization*; Office of Science, U.S. Department of Energy: Washington, DC, 2005.
(2) Lewis, N. S.; Nocera, D. G. *Proc. Natl. Acad. Sci. U.S.A.* **2006**, *103*, 15729–15735.
(3) Alstrum-Acevedo, J. H.; Brennaman, M. K.; Meyer, T. J. *Inorg. Chem.* **2005**, *44*, 6802–6827.
(4) Ardo, S.; Meyer, G. J. *Chem. Soc. Rev.* **2009**, *38*, 115–164.
(5) Balzani, V.; Credi, A.; Venturi, M. *ChemSusChem* **2008**, *1*, 26–58.
(6) O'Regan, B.; Gratzel, M. *Nature* **1991**, *353*, 737–740.
(7) Martinson, A. B. F.; Hamann, T. W.; Pellin, M. J.; Hupp, J. T. *Chem.—Eur. J.* **2008**, *14*, 4458–4467.
(8) Brabec, C. J.; Sariciftci, N. S.; Hummelen, J. C. *Adv. Funct. Mater.* **2001**, *11*, 15–26.
(9) Coakley, K. M.; McGehee, M. D. *Chem. Mater.* **2004**, *16*, 4533–4542.
(10) Gledhill, S.; Scott, B.; Gregg, B. *J. Mater. Res.* **2005**, *20*, 3167–3179.
(11) Hoppe, H.; Sariciftci, N. *J. Mater. Res.* **2004**, *19*, 1924–1945.
(12) Wasielewski, M. R. *J. Org. Chem.* **2006**, *71*, 5051–5066.
(13) Gust, D.; Moore, T. A.; Moore, A. L. *Acc. Chem. Res.* **2001**, *34*, 40–48.
(14) Albinsson, B.; Eng, M.; Pettersson, K.; Winters, M. *Phys. Chem. Chem. Phys.* **2007**, *9*, 5847.

Published on Web 10/26/2009

Scheme 1. Design Scheme for Conformational Manipulation of ET Rate Constants and Trapping of Charge-Separated Equivalents

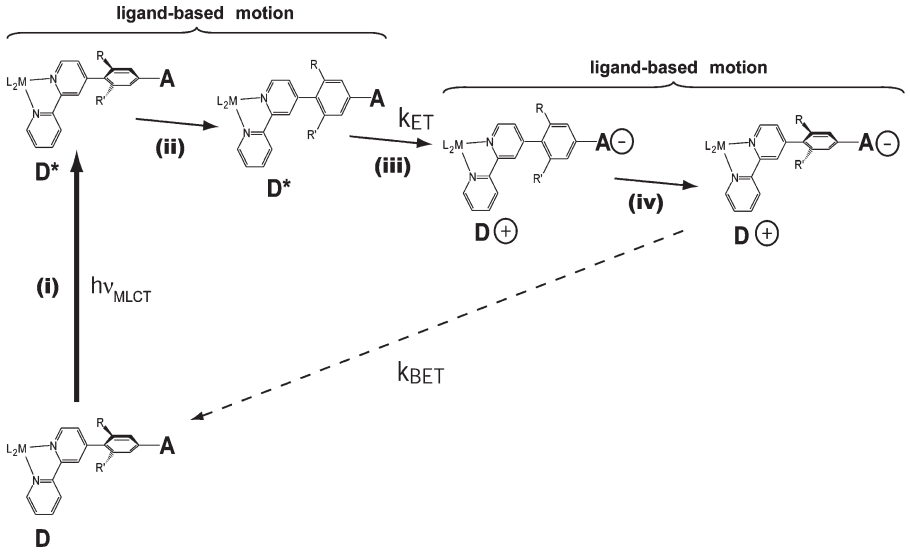

wasting reverse ET events utilizing common coupling pathways can begin to compete with productive events. One strategy to be refined and exploited involves the deliberate use of additional nuclear coordinates, secondary to the ET events themselves, as a means of altering electronic coupling, reorganization energy, and reaction free energy, each of which influences the kinetics of charge separation. An example of this is proton-coupled ET reactions critical for solar energy conversion to fuels.[15,16] Here we consider torsional motions in multicomponent π-systems. Understanding the role of such motions for controlling ET, exchange-mediated energy transfer, and conduction in molecular and material systems is a burgeoning field of research motivated by the idea that low frequency modes of this nature can have a major impact on intercomponent electronic coupling.[14,17−51] This paper is a continuation of efforts in our group to explore how metal-to-ligand charge-transfer (MLCT) initiated aryl-ring rotation motions within Ru^{II} DA systems of our design might assist productive ET events and how the reverse motions can be harnessed to hinder energy wasting charge recombination. We have recently published experimental work on prototype systems built from asymmetric aryl-substituted bipyridine ligands where the goal was to make strides toward molecular conformational switching of ET rates according to Scheme 1.[50]

The initial step here involves MLCT excitation of the donor portion of the DA system. Charge is formally transferred from the metal center to the π^* system of what is initially (according to the ground state geometry) a non-coplanar ligand-aryl structure. In step (**ii**) intraligand electronic delocalization involving the charge-transferred

(15) Huynh, M. H. V.; Meyer, T. *J. Chem. Rev.* **2007**, *107*, 5004–5064.
(16) Reece, S. Y.; Nocera, D. G. *Annu. Rev. Biochem.* **2009**, *78*, 673–699.
(17) Larsson, S. *J. Am. Chem. Soc.* **1981**, *103*, 4034–4040.
(18) Helms, A.; Heiler, D.; McLendon, G. *J. Am. Chem. Soc.* **1991**, *113*, 4325–4327.
(19) Gourdon, A. *New J. Chem.* **1992**, *16*, 953–957.
(20) Dong, T. Y.; Huang, C. H.; Chang, C. K.; Wen, Y. S.; Lee, S. L.; Chen, J. A.; Yeh, W. Y.; Yeh, A. *J. Am. Chem. Soc.* **1993**, *115*, 6357–6368.
(21) Ward, M. D. *Chem. Soc. Rev.* **1995**, *24*, 121–134.
(22) Sachs, S. B.; Dudek, S. P.; Hsung, R. P.; Sita, L. R.; Smalley, J. F.; Newton, M. D.; Feldberg, S. W.; Chidsey, C. E. D. *J. Am. Chem. Soc.* **1997**, *119*, 10563.
(23) Newton, M. D. *Int. J. Quantum Chem.* **2000**, *77*, 255–263.
(24) Toutounji, M. M.; Ratner, M. A. *J. Phys. Chem. A* **2000**, *104*, 8566–8569.
(25) Davis, W. B.; Ratner, M. A.; Wasielewski, M. R. *J. Am. Chem. Soc.* **2001**, *123*, 7877–7886.
(26) Nelsen, S. F.; Li, G. Q.; Konradsson, A. *Org. Lett.* **2001**, *3*, 1583–1586.
(27) Nelsen, S. F.; Blomgren, F. *J. Org. Chem.* **2001**, *66*, 6551–6559.
(28) Kyrychenko, A.; Albinsson, B. *Chem. Phys. Lett.* **2002**, *366*, 291–299.
(29) Johansson, O.; Borgstrom, M.; Lomoth, R.; Palmblad, M.; Bergquist, J.; Hammarstrom, L.; Sun, L. C.; Akermark, B. *Inorg. Chem.* **2003**, *42*, 2908–2918.
(30) Benniston, A. C.; Harriman, A.; Li, P.; Sams, C. A.; Ward, M. D. *J. Am. Chem. Soc.* **2004**, *126*, 13630.
(31) Rubtsov, I. V.; Redmore, N. P.; Hochstrasser, R. M.; Therien, M. J. *J. Am. Chem. Soc.* **2004**, *126*, 2684–2685.
(32) Joachim, C.; Ratner, M. A. *Nanotechnology* **2004**, *15*, 1065–1075.
(33) Smalley, J. F.; Sachs, S. B.; Chidsey, C. E. D.; Dudek, S. P.; Sikes, H. D.; Creager, S. E.; Yu, C. J.; Feldberg, S. W.; Newton, M. D. *J. Am. Chem. Soc.* **2004**, *126*, 14620.
(34) Benniston, A. C.; Harriman, A.; Li, P. Y.; Patel, P. V.; Sams, C. A. *Phys. Chem. Chem. Phys.* **2005**, *7*, 3677–3679.
(35) Holman, M. W.; Yan, P.; Ching, K. C.; Liu, R. C.; Ishak, F. I.; Adams, D. M. *Chem. Phys. Lett.* **2005**, *413*, 501–505.
(36) Weiss, E. A.; Tauber, M. J.; Kelley, R. F.; Ahrens, M. J.; Ratner, M. A.; Wasielewski, M. R. *J. Am. Chem. Soc.* **2005**, *127*, 11842–11850.
(37) Welter, S.; Salluce, N.; Belser, P.; Groeneveld, M.; De Cola, L. *Coord. Chem. Rev.* **2005**, *249*, 1360–1371.
(38) Valasek, M.; Pecka, J.; Jindrich, J.; Calleja, G.; Craig, P. R.; Michl, J. *J. Org. Chem.* **2005**, *70*, 405–412.
(39) Benniston, A. C.; Harriman, A. *Chem. Soc. Rev.* **2006**, *35*, 169–179.
(40) Benniston, A. C.; Harriman, A.; Li, P. Y.; Patel, P. V.; Sams, C. A. *J. Org. Chem.* **2006**, *71*, 3481–3493.
(41) Eng, M. P.; Ljungdahl, T.; Martensson, J.; Albinsson, B. *J. Phys. Chem. B* **2006**, *110*, 6483–6491.
(42) Laine, P. P.; Bedioui, F.; Loiseau, F.; Chiorboli, C.; Campagna, S. *J. Am. Chem. Soc.* **2006**, *128*, 7510–7521.
(43) Laine, P. P.; Loiseau, F.; Campagna, S.; Ciofini, I.; Adamo, C. *Inorg. Chem.* **2006**, *45*, 5538–5551.
(44) Venkataraman, L.; Klare, J. E.; Nuckolls, C.; Hybertsen, M. S.; Steigerwald, M. L. *Nature* **2006**, *442*, 904–907.
(45) Indelli, M. T.; Chiorboli, C.; Flamigni, L.; De Cola, L.; Scandola, F. *Inorg. Chem.* **2007**, *46*, 5630–5641.
(46) Weber, J. M.; Rawls, M. T.; MacKenzie, V. J.; Limoges, B. R.; Elliott, C. M. *J. Am. Chem. Soc.* **2007**, *129*, 313–320.
(47) Albinsson, B.; Martensson, J. *J. Photochem. Photobiol., C* **2008**, *9*, 138–155.
(48) Benniston, A.; Harriman, A.; Li, P.; Patel, P.; Sams, C. *Chem.—Eur. J.* **2008**, *14*, 1710–1717.
(49) Laine, P. P.; Campagna, S.; Loiseau, F. *Coord. Chem. Rev.* **2008**, 2552–2571.
(50) Meylemans, H.; Lei, C. F.; Damrauer, N. H. *Inorg. Chem.* **2008**, *47*, 460–476.
(51) Eng, M. P.; Albinsson, B. *Chem. Phys.* **2009**, *357*, 132–139.

electron in the triplet state manifold of the molecule drives inter-ring rotation motions. These are then expected to alter nuclear and electronic properties tied to the forward ET in step (**iii**). Once ET to the acceptor is complete, inter-ring steric interactions between components of the aryl substituent and bipyridine ligand are expected to drive the reformation of a non-coplanar inter-ring geometry (step (**iv**)). This is a critical step that is hypothesized to reduce electronic coupling between the useful charge separated state and the ground state that would be re-formed by energy-wasting back ET. In our published work[50] and recent follow-up experiments, we observe driving-force insensitivity in forward ET rate constants for three DA systems containing the same aryl-substituted bipyridine ligand but different ancillary ligands, L (bpy, dmb, and tmb where bpy = 2,2′-bipyridine, dmb = 4,4′-dimethyl-2,2′-bipyridine, and tmb = 4,4′,5,5′-tetramethyl-2,2′-bipyridine). Our explanation invokes the reduction of reorganization energy due to ring-rotation motions represented by step **ii**. Experimental work has not yet been published that supports or refutes the reverse switching in step **iv**. The aim of this computational work is to consider the validity of the model presented in Scheme 1 with respect to the various conformational changes.

Excited state intraligand electron delocalization following photoexcitation of transition metal complexes has been explored or implicated in a variety of systems.[29,42,49,50,52−73] It was initially used by McMillin to explain large MLCT extinction coefficients in Cu^{I} systems and by inference related Ru^{II} systems having aryl-substituted polypyridine ligands.[52] Through work by Meyer and co-workers it became a useful paradigm to understand photophysical properties such as increased radiative quantum yields and emission lifetimes in metal complexes having ligands with extended π-systems involved in the thermalized MLCT state.[53,56,57] The basic idea being that delocalization of the charge-transferred electron over a larger ligand-based π-system has the effect of diminishing vibrational overlap between the lowest energy vibrational levels of the ^{3}MLCT state and isoenergetic highly excited vibrational levels of the ground state (the states become more nested) thus reducing Franck−Condon factors and therefore rates of non-radiative decay. The possibility for excited-state ring rotation motions preceding intraligand electron delocalization was considered by McCusker's group using structural, photophysical, electrochemical, computational, and ultrafast transient absorption studies of metal complexes having 4,4′-diaryl-2,2′-bipyridine ligands with different amounts of steric repulsion between the aryl and bipyridine fragments.[58,60,62,63] For molecules such as $[Ru(dpb)3]^{2+}$ (where dpb = 4,4′-diphenyl-2,2′-bipyridine) in room temperature acetonitrile, a key observation was transient growth, on a ∼1 ps time scale, of spectral signatures attributed to a ligand-based radical anion in the extended π-system. Similar transient signals have been observed in other systems and are afforded the same mechanistic interpretation.[42,50] It is possible they contribute to ultrafast transient absorptions signals recently observed in Cu^{I} systems with aryl-substituted phenanthroline ligands; however, spectra and kinetics there are very rich in part because of transient Jahn−Teller distortion of the coordination geometry itself and contributions from intraligand electronic delocalization have not been specifically identified.[74]

While experimental support of excited-state intraligand electron delocalization following MLCT is extensive, computational evidence, especially that which confirms the aforementioned ring-rotation dynamical picture following MLCT, is less unified. McCusker and co-workers provided support for ligand-based dynamics with a model that compared gas-phase HF, MP2, and DFT structures of 4-phenylpyiridine with its radical anion.[60] They showed that the one-electron reduced system has an inter-ring dihedral angle of 0° which is ∼45° less than the neutral system. On the other hand Baranovski and Lyubimova, in a HF study of 4,4′-diphenyl-2,2′-bipyridine and its one-electron reduced form, only observed a −4.3° change in the aryl-to-bpy dihedral angle.[75] While we do not agree with their interpretation, they claim this is a result of steric interactions between phenyl substituents at the 4 and 4′ positions of the same bipyridine ligand. Adamo and Laine have applied density functional theory (DFT) to, among other things, bis-homoleptic Ru^{II} and Os^{II} metal complexes containing two 4′-p-tolyl-2,2′;6′,2″-terpyridine ligands. Upon reduction of these species (for both metals) they observe an increase of 2° in the aryl-terpyridine

(52) Phifer, C. C.; McMillin, D. R. *Inorg. Chem.* **1986**, *25*, 1329–1333.
(53) Boyde, S.; Strouse, G. F.; Jones, W. E.; Meyer, T. J. *J. Am. Chem. Soc.* **1990**, *112*, 7395–7396.
(54) Collin, J. P.; Guillerez, S.; Sauvage, J. P.; Barigelletti, F.; Decola, L.; Flamigni, L.; Balzani, V. *Inorg. Chem.* **1991**, *30*, 4230–4238.
(55) Sauvage, J. P.; Collin, J. P.; Chambron, J. C.; Guillerez, S.; Coudret, C.; Balzani, V.; Barigelletti, F.; Decola, L.; Flamigni, L. *Chem. Rev.* **1994**, *94*, 993–1019.
(56) Strouse, G. F.; Schoonover, J. R.; Duesing, R.; Boyde, S.; Jones, W. E.; Meyer, T. J. *Inorg. Chem.* **1995**, *34*, 473–487.
(57) Treadway, J. A.; Loeb, B.; Lopez, R.; Anderson, P. A.; Keene, F. R.; Meyer, T. J. *Inorg. Chem.* **1996**, *35*, 2242–2246.
(58) Damrauer, N. H.; Boussie, T. R.; Devenney, M.; McCusker, J. K. *J. Am. Chem. Soc.* **1997**, *119*, 8253–8268.
(59) Hammarstrom, L.; Barigelletti, F.; Flamigni, L.; Indelli, M. T.; Armaroli, N.; Calogero, G.; Guardigli, M.; Sour, A.; Collin, J. P.; Sauvage, J. P. *J. Phys. Chem. A* **1997**, *101*, 9061–9069.
(60) Damrauer, N. H.; Weldon, B. T.; McCusker, J. K. *J. Phys. Chem. A* **1998**, *102*, 3382–3397.
(61) Feliz, M. R.; Rodriguez-Nieto, F.; Ruiz, G.; Wolcan, E. *J. Photochem. Photobiol., A* **1998**, *117*, 185.
(62) Damrauer, N. H.; McCusker, J. K. *Inorg. Chem.* **1999**, *38*, 4268–4277.
(63) Damrauer, N. H.; McCusker, J. K. *J. Phys. Chem. A* **1999**, *103*, 8440–8446.
(64) Miller, M. T.; Gantzel, P. K.; Karpishin, T. B. *Inorg. Chem.* **1999**, *38*, 3414.
(65) Michalec, J. F.; Bejune, S. A.; McMillin, D. R. *Inorg. Chem.* **2000**, *39*, 2708 ff.
(66) Berg, K. E.; Tran, A.; Raymond, M. K.; Abrahamsson, M.; Wolny, J.; Redon, S.; Andersson, M.; Sun, L. C.; Styring, S.; Hammarstrom, L.; Toftlund, H.; Akermark, B. *Eur. J. Inorg. Chem.* **2001**, 1019–1029.
(67) Michalec, J. F.; Bejune, S. A.; Cuttell, D. G.; Summerton, G. C.; Gertenbach, J. A.; Field, J. S.; Haines, R. J.; McMillin, D. R. *Inorg. Chem.* **2001**, *40*, 2193–2200.
(68) Walters, K. A.; Ley, K. D.; Cavalaheiro, C. S. P.; Miller, S. E.; Gosztola, D.; Wasielewski, M. R.; Bussandri, A. P.; van Willigen, H.; Schanze, K. S. *J. Am. Chem. Soc.* **2001**, *123*, 8329–8342.
(69) Walters, K. A.; Premvardhan, L. L.; Liu, Y.; Peteanu, L. A.; Schanze, K. S. *Chem. Phys. Lett.* **2001**, *339*, 255–262.
(70) Wang, Y. S.; Liu, S. X.; Pinto, M. R.; Dattelbaum, D. M.; Schoonover, J. R.; Schanze, K. S. *J. Phys. Chem. A* **2001**, *105*, 11118–11127.
(71) Balazs, G. C.; del Guerzo, A.; Schmehl, R. H. *Photochem. Photobiol. Sci.* **2005**, *4*, 89–94.
(72) Goze, C.; Sabatini, C.; Barbieri, A.; Barigelletti, F.; Ziessel, R. *Inorg. Chem.* **2007**, *46*, 7341–7350.
(73) Clark, M. L.; Diring, S.; Retailleau, P.; McMillin, D. R.; Ziessel, R. *Chem.—Eur. J.* **2008**, *14*, 7168–7179.
(74) Shaw, G. B.; Grant, C. D.; Shirota, H.; Castner, E. W.; Meyer, G. J.; Chen, L. X. *J. Am. Chem. Soc.* **2007**, *129*, 2147–2160.
(75) Lyubimova, O. O.; Baranovskii, V. I. *Zh. Strukt. Khim.* **2003**, *44*, 728–735.

Scheme 2. Systems and Geometrical Parameters under Consideration Herein

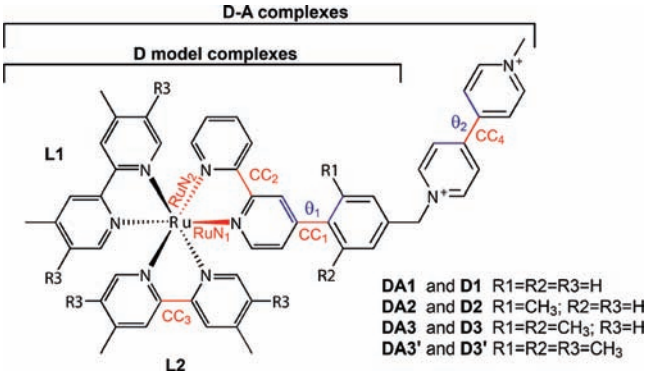

dihedral angle.[76] In subsequent studies of related bis-heteroleptic Os^{II} complexes, where one of the two aryl-substituted terpyridine ligands is covalently bound to an electron withdrawing triphenyl-pyridinium moiety, a −13° change in the aryl-terpyridine dihedral angle is observed upon metal complex reduction (from 36.7° to 23.4°).[43] Similar to our approach here, these workers also considered structural changes in the comparison between the lowest energy triplet of the complex and its ground state. In this case they observe a −10° change in the aryl-terpyridine dihedral angle from 36.7° in the ground state to 26.9° in the lowest energy triplet.

This disparate collection of predictions for aryl-polypyridyl dihedral angle changes in models of thermalized MLCT states relative to ground states suggests that the energetic driving forces behind such torsional conformational changes may be subtle and system specific. This paper aims to address cases relevant to Scheme 1 with a focus on demonstrating consistency with several density functionals common in the literature. The systems and main geometrical parameters under investigation here can be summarized in Scheme 2.

We first consider ground state geometries of full donor−acceptor species as a function of the degree of steric hindrance (groups R1 and R2 in Scheme 2) between the aryl substituent and the bipyridine fragment. We then explore conformational changes that might ensue in step **ii** (Scheme 1) with a variety of ^{3}MLCT models. Finally we address reverse conformational changes (step **iv**) in $^3D^+-A^-$ models and address the role of solvation in determining the torsional conformation of these species.

Computational Methods

DFT electronic structure calculations were carried out using the Gaussian03 software package.[77] Geometry optimizations were undertaken using several different exchange and correlation functional models to investigate whether there are any significant variations in calculated geometry as a function of method. For all compounds and spin states, three different hybrid Hartree−Fock/density functional models (HF/DFT) were used. The first of these B3LYP combines Becke's 3-parameter hybrid exchange (B3) with the nonlocal correlation functional of Lee, Yang, and Parr (LYP).[78,79] B3LYP was chosen as it is one of the most widely used functional models for transition metal complexes.[80−83] The second B3PW91 combines Becke's 3-parameter hybrid exchange (B3) with the correlation functional Perdew−Wang-91.[78,84] This particular functional model was chosen as it has been shown to give more accurate bond lengths when compared with B3LYP and PBE0 functionals.[81,83] The third is PBE1PBE, also known as PBE0, which is obtained by casting the functional and correlation of Perdew, Burke and Erzenrhof in a hybrid HF/DFT scheme with a fixed 1/4 ratio.[85−87] This functional has been shown to improve the accuracy of excitation energies and charge transfer bands in metal complexes for both gas phase and solution calculations.[88−92] Unless noted, geometries were optimized with no constraints. Coordinates are available in Supporting Information for each B3LYP optimized structure. For ruthenium atoms the LANL2DZ[93] basis set was used along with the corresponding pseudopotential for the metal atom while C, H, and N were treated with 6-31G.

Ground-state species (energy and geometry) were modeled with the lowest-energy singlet calculated with restricted methods. MLCT excited states of donor complexes and charge separated states of donor−acceptor complexes were modeled with the lowest-energy triplet determined using unrestricted methods. For these, spin contamination was found to be negligible based on the expectation values of the total spin angular momentum operator S^2. All gas phase geometry optimizations using the B3LYP functional were followed by calculation of analytical vibrational frequencies. Only positive real frequencies were observed indicating that these structures are stationary minima. It is noted that for species **D2** and **DA2** there are two different conformers where the ortho-methyl substituent on the aryl group points either inward or outward with respect to the central C−C bond of the asymmetric bipyridine. We tested the energy difference between such conformers using the B3LYP functional and

(76) Ciofini, I.; Laine, P. P.; Bedioui, F.; Adamo, C. *J. Am. Chem. Soc.* **2004**, *126*, 10763–10777.
(77) Frisch, M. J.; Trucks, G. W.; Schlegel, H. B.; Scuseria, G. E.; Robb, M. A.; Cheeseman, J. R.; Montgomery, J. J. A.; Vreven, T.; Kudin, K. N.; Burant, J. C.; Millam, J. M.; Iyengar, S. S.; Tomasi, J.; Barone, V.; Mennucci, B.; Cossi, M.; Scalmani, G.; Rega, N.; Petersson, G. A.; Nakatsuji, H.; Hada, M.; Ehara, M.; Toyota, K.; Fukuda, R.; Hasegawa, J.; Ishida, M.; Nakajima, T.; Honda, Y.; Kitao, O.; Nakai, H.; Klene, M.; Li, X.; Knox, J. E.; Hratchian, H. P.; Cross, J. B.; Bakken, V.; Adamo, C.; Jaramillo, J.; Gomperts, R.; Stratmann, R. E.; Yazyev, O.; Austin, A. J.; Cammi, R.; Pomelli, C.; Ochterski, J. W.; Ayala, P. Y.; Morokuma, K.; Voth, G. A.; Salvador, P.; Dannenberg, J. J.; Zakrzewski, V. G.; Dapprich, S.; Daniels, A. D.; Strain, M. C.; Farkas, O.; Malick, D. K.; Rabuck, A. D.; Raghavachari, K.; Foresman, J. B.; Ortiz, J. V.; Cui, Q.; Baboul, A. G.; Clifford, S.; Cioslowski, J.; Stefanov, B. B.; Liu, G.; Liashenko, A.; Piskorz, P.; Komaromi, I.; Martin, R. L.; Fox, D. J.; Keith, T.; Al-Laham, M. A.; Peng, C. Y.; Nanayakkara, A.; Challacombe, M.; Gill, P. M. W.; Johnson, B.; Chen, W.; Wong, M. W.; Gonzalez, C.; Pople, J. A. *Gaussian 03*, Revision D.01; Gaussian, Inc.: Pittsburgh, PA, 2004.
(78) Becke, A. D. *J. Chem. Phys.* **1993**, *98*, 5648–5652.
(79) Lee, C. T.; Yang, W. T.; Parr, R. G. *Phys. Rev. B: Condens. Matter* **1988**, *37*, 785–789.
(80) Vlcek, A.; Zalis, S. *Coord. Chem. Rev.* **2007**, *251*, 258–287.
(81) Buhl, M.; Reimann, C.; Pantazis, D. A.; Bredow, T.; Neese, F. *J. Chem. Theory Comput.* **2008**, *4*, 1449–1459.
(82) Rinaldo, D.; Tian, L.; Harvey, J. N.; Friesner, R. A. *J. Chem. Phys.* **2008**, *129*, 23.
(83) Kelly, C. P.; Cramer, C. J.; Truhlar, D. G. *J. Chem. Theory Comput.* **2005**, *1*, 1133–1152.
(84) Perdew, J. P.; Wang, Y. *Phys. Rev. B* **1992**, *45*, 13244–13249.
(85) Adamo, C.; Barone, V. *J. Chem. Phys.* **1999**, *110*, 6158–6170.
(86) Perdew, J. P.; Burke, K.; Ernzerhof, M. *Phys. Rev. Lett.* **1996**, *77*, 3865–3868.
(87) Perdew, J. P.; Burke, K.; Ernzerhof, M. *Phys. Rev. Lett.* **1997**, *78*, 1396–1396.
(88) Adamo, C.; Barone, V. *Theor. Chem. Acc.* **2000**, *105*, 169–172.
(89) Barone, V.; de Biani, F. F.; Ruiz, E.; Sieklucka, B. *J. Am. Chem. Soc.* **2001**, *123*, 10742–10743.
(90) Guillemoles, J. F.; Barone, V.; Joubert, L.; Adamo, C. *J. Phys. Chem. A* **2002**, *106*, 11354–11360.
(91) Ciofini, I. *Theor. Chem. Acc.* **2006**, *116*, 219–231.
(92) Rekhis, M.; Labat, F.; Ouamerali, O.; Ciofini, I.; Adamo, C. *J. Phys. Chem. A* **2007**, *111*, 13106–13111.
(93) Hay, P. J.; Wadt, W. R. *J. Chem. Phys.* **1985**, *82*, 299–310.

Table 1. Energy and Structural Properties of the Ground State Singlet for $[Ru(dmb)_2(bpy\text{-}\phi\text{-}MV)]^{4+}$ (**DA1**), $[Ru(dmb)_2(bpy\text{-}o\text{-}tolyl\text{-}MV)]^{4+}$ (**DA2**), $[Ru(dmb)_2(bpy\text{-}2,6\text{-}Me_2\text{-}\phi\text{-}MV)]^{4+}$ (**DA3**), and $[Ru(tmb)_2(bpy\text{-}2,6\text{-}Me_2\text{-}\phi\text{-}MV)]^{4+}$ (**DA3′**) Optimized in the Gas Phase[a,b]

method B3LYP	**DA1** (L = dmb)	**DA2** (L = dmb)	**DA3** (L = dmb)	**DA3′** (L = tmb)
energy (hartree)	−2540.8162	−2580.1222	−2619.4297	−2776.6763
θ_1 (av)	34.6°	49.9°	85.5	85.9°
θ_2 (av)	39.5°	38.7°	38.7°	39.0°
CC_1	1.489 Å	1.495 Å	1.501 Å	1.505 Å
CC_2	1.472 Å	1.472 Å	1.471 Å	1.471 Å
CC_3	1.474 Å	1.474 Å	1.474 Å	1.471 Å
CC_4	1.490 Å	1.490 Å	1.490 Å	1.490 Å
RuN_1	2.104 Å	2.110 Å	2.110 Å	2.110 Å
RuN_2	2.105 Å	2.106 Å	2.106 Å	2.103 Å

[a] For all calculations the basis set for Ru was LANL2DZ with an ECP and 631-G for all N, C and H atoms. [b] See Supporting Information, Table S1 for comparative results from calculations run using the B3LYP, B3PW91, and PBE1PBE functionals.

D2* (the lowest energy triplet, vide infra). The energies agree to within 0.03 kcal/mol (0.0013 eV) so this issue is not considered further.

To determine the amount of energy released in the formation of a geometry-relaxed ^{3}MLCT state from hypothetical singlet Franck−Condon state, single point calculations were run using relevant properties of ground state geometries. There is a subtle complication because our ground state geometries contain an electroactive MV^{2+} moiety whereas the ^{3}MLCT models do not. To account for this the methyl viologen acceptor unit was removed (holding the geometry of the metal complex including the methylene in a fixed geometry) and the C−N bond was replaced with a C−H bond fixed at the default Gaussian software bond length. In general the structures were not optimized with respect to this single bond or the angles and dihedral angles of the new methyl substituent. However, this is energetically negligible: in one case where we did allow the methyl substituent to optimize while holding other geometrical parameters fixed, only 0.001 kcal/mol (4.3×10^{-5} eV) were gained. As discussed in the manuscript there are several instances where electronic structure was modeled with a self-consistent reaction field (SCRF) with the use of a polarizable continuum model (PCM) using the dielectric for acetonitrile.[94,95]

This research was supported in part by the National Science Foundation through TeraGrid resources provided by the National Center for Supercomputing Applications with all computations performed on the Cobalt computer cluster.[96]

Results and Discussion

Ground State DA Geometries. In coupled aryl systems within organic compounds and coordination complexes it is common to observe non-coplanar ring structures which arise as the stabilizing effects of π-system delocalization balance with steric repulsions between substituents ortho to the bond of inter-ring coupling. This is true even when those substituents are hydrogen atoms. For example, the inter-ring dihedral angle for neutral biphenyl in the gas phase has been measured[97] and calculated[35,98] to be on the order of 38°−44°. In work by McCusker and co-workers 4-phenylpyridine was used as a computational model for a symmetric phenyl substituted bipyridine ligand. Using MP2 calculations in the gas phase they reported an inter-ring dihedral of 44.6° which is comparable to those found in biphenyl.[60] In addition to studies of free ligand geometries there have also been a number of experimental and computational studies exploring the structure of aryl substituted polypyridyl transition metal complexes. X-ray structures have been reported for systems with different transition metal centers including Fe,[99] Ru,[58,70,100−106] Os,[107] Pt,[108−110] Mn,[111] and Cu.[112] While there are on the order of 10's of crystal structures reported for these types of examples, computational systems are limited to only a handful,[43,76,91,113] most notably the work of Adamo, Laine, and co-workers.

Tables 1 and Supporting Information, Table S1 presents energetic and structural information calculated for the four ground state DA species as gas-phase molecules. Regarding **DA1**, where the source of steric influence is from hydrogen atoms, an inter-ring dihedral angle (θ_1) of ~35° is observed. There is excellent agreement in θ_1 and θ_2 across hybrid functionals (see Supporting Information, Table S1). In terms of θ_1 which is critical to our model of conformational switching, the largest variation that is seen is 1.2° in the comparison of B3LYP versus B3PW91. Such a difference is significantly less than the modeled conformational changes of the excited state (vide infra). There is also very little variation in structural information pertaining to C−C bond distances as a function of method. The largest variation for CC_1, CC_2, CC_3, and CC_4 occurs between PBE1PBE and B3LYP with the former consistently predicting a bond length

(94) Tomasi, J.; Mennucci, B.; Cammi, R. *Chem. Rev.* **2005**, *105*, 2999–3093.
(95) Cances, E.; Mennucci, B.; Tomasi, J. *J. Chem. Phys.* **1997**, *107*, 3032–3041.
(96) Catlett, C. et. al. *HPC and Grids in Action; Advances in Parallel Computing,* **2007**.
(97) Almenningen, A.; Bastiansen, O.; Fernholt, L.; Cyvin, B. N.; Cyvin, S. J.; Samdal, S. *J. Mol. Struct.* **1985**, *128*, 59–76.
(98) Rubio, M.; Merchan, M.; Orti, E.; Roos, B. O. *J. Phys. Chem.* **1995**, *99*, 14980.
(99) Krass, H.; Plummer, E. A.; Haider, J. M.; Barker, P. R.; Alcock, N. W.; Pikramenou, Z.; Hannon, M. J.; Kurth, D. G. *Angew. Chem., Int. Ed.* **2001**, *40*, 3862 ff.
(100) Bushell, K. L.; Couchman, S. M.; Jeffery, J. C.; Rees, L. H.; Ward, M. D. *J. Chem. Soc., Dalton Trans.* **1998**, 3397–3403.
(101) Alcock, N. W.; Barker, P. R.; Haider, J. M.; Hannon, M. J.; Painting, C. L.; Pikramenou, Z.; Plummer, E. A.; Rissanen, K.; Saarenketo, P. *J. Chem. Soc., Dalton Trans.* **2000**, *9*, 1447–1461.
(102) Barigelletti, F.; Ventura, B.; Collin, J. P.; Kayhanian, R.; Gavina, P.; Sauvage, J. P. *Eur. J. Inorg. Chem.* **2000**, 113–119.
(103) Bonnet, S.; Collin, J. P.; Gruber, N.; Sauvage, J. P.; Schofield, E. R. *Dalton Trans.* **2003**, 4654–4662.
(104) Bonnet, S.; Collin, J. P.; Sauvage, J. P.; Schofield, E. *Inorg. Chem.* **2004**, *43*, 8346–8354.
(105) Abrahamsson, M.; Wolpher, H.; Johansson, O.; Larsson, J.; Kritikos, M.; Eriksson, L.; Norrby, P. O.; Bergquist, J.; Sun, L. C.; Akermark, B.; Hammarstrom, L. *Inorg. Chem.* **2005**, *44*, 3215–3225.
(106) Cooke, M. W.; Hanan, G. S.; Loiseau, F.; Campagna, S.; Watanabe, M.; Tanaka, Y. *J. Am. Chem. Soc.* **2007**, *129*, 10479–10488.
(107) Lai, S. W.; Chan, Q. K. W.; Zhu, N.; Che, C. M. *Inorg. Chem.* **2007**, *46*, 11003–11016.
(108) Field, J. S.; Gertenbach, J. A.; Haines, R. J.; Ledwaba, L. P.; Mashapa, N. T.; McMillin, D. R.; Munro, O. Q.; Summerton, G. C. *Dalton Trans.* **2003**, 1176–1180.
(109) Okamura, R.; Wada, T.; Aikawa, K.; Nagata, T.; Tanaka, K. *Inorg. Chem.* **2004**, *43*, 7210–7217.
(110) Sakamoto, R.; Murata, M.; Kume, S.; Sampei, H.; Sugimoto, M.; Nishihara, H. *Chem. Commun.* **2005**, 1215–1217.
(111) Chen, H. Y.; Tagore, R.; Das, S.; Incarvito, C.; Faller, J. W.; Crabtree, R. H.; Brudvig, G. W. *Inorg. Chem.* **2005**, *44*, 7661–7670.
(112) Storrier, G. D.; Colbran, S. B.; Craig, D. C. *J. Chem. Soc., Dalton Trans.* **1998**, 1351–1363.
(113) Polson, M.; Ravaglia, M.; Fracasso, S.; Garavelli, M.; Scandola, F. *Inorg. Chem.* **2005**, *44*, 1282–1289.

0.006 Å shorter than the latter. With respect to RuN_1 and RuN_2 distances, predictions by the B3PW91 and PBE1PBE functional models are in very close agreement and predict slightly smaller (~0.02 Å−0.03 Å) bond distances than the B3LYP functional. Considering the agreement among density functional models for C−C bond lengths and considering that we do not vary the basis sets that have been used, these observations point to subtle differences in how the functionals treat metal ligand bonding. Understanding why this is the case is beyond the scope of this paper. However, it is stressed that the total deviation in both RuN_1 and RuN_2 as the functional is changed is still very small and represents less than 1% of each respective bond length.

Our calculated θ_1 are in good agreement with computational explorations of coordination complexes with similar structural motifs reported in the literature. For example, in investigations of 4′-aryl-substituted terpyridine complexes of Ru^{II} and Os^{II}, Adamo, Laine, and coworkers reported inter-ring dihedral angles (related to our θ_1) of 30.5° and 30.6°, respectively, using the PBE0 functional (equivalent to Gaussian's implementation of PBE1PBE).[76] In their related calculations of an asymmetric donor−acceptor complex involving Os^{II} where one aryl-substituted terpyridine ligand is attached to a triphenyl-pyridinium acceptor (attached) and one is not (ancillary), they see inter-ring dihedral angles (again related to our θ_1) of 35.9° (attached) and 29.3° (ancillary).[76] Very similar results were reported by Adamo and Laine for several structurally and electronically related Os^{II} systems also using the PBE0 functional.[43] Additionally, there are computational results available for 4′-aryl-substituted terpyridyl iridium systems. These systems were investigated using B3LYP, which resulted in the pendant phenyl ring being twisted out of the plane by 36 ± 1°. These workers were able to compare their computational structure with crystallographic data and found excellent agreement with torsions as well as bond lengths.[113]

Comparisons with experimental structural results would also be very useful in assessing the accuracy of our calculations. Unfortunately, X-ray quality crystals for **DA1** and **D1** are as of yet unavailable. However, there are known structures involving aryl-substituted polypyridyl bidentate and tridentate ligands of Ru^{II} for comparison. If we consider only cases with hydrogen atom substituents ortho to the aryl-polypyridyl coupling, then there are ~25 well ordered instances of aryl-polypyridyl-Ru^{2+} moieties within 21 separate X-ray structures where the aryl groups have either no substituents (i.e., C_6H_5) or have alkyl substituents at para or meta positions.[58,100,102−105,114−122] Within this set the relevant dihedral angle (comparable to θ_1) ranges from 6°−42° with an average of 24° and a standard deviation of 10°. The broad distribution suggests that this is very likely a soft potential and that crystal packing forces may play a significant role in the variation in this dihedral angle.[58,123] Within this set there are only two structures with aryl-substituted bipyridine ligands complexed to Ru^{II},[58,121] and both of these have the ligand dpb. For these two structures the average Ru−N bond distance (comparable to our $Ru-N_1$) is 2.055 Å with a standard deviation of 0.006 Å. The other structures involve aryl-substituted terpyridine ligands of Ru^{II} with significantly shorter Ru−N bond distances on the central pyridine ring (the average of 21 instances is 1.97 Å with a standard deviation of 0.03 Å). Comparing the aryl-substituted bipyridine "$Ru-N_1$" average to our computed value for **DA1** (2.104 Å for B3LYP, 2.079 Å for B3PW91, 2.074 Å for PBE1PBE) it is seen that DFT methods we used overestimate the Ru−N bond length by 0.049 Å−0.019 Å with B3PW91 and PBE1PBE faring better than B3LYP. The overestimation is consistent with published results from similar systems where it has been shown that the Ru−N bond distances are generally overestimated with DFT involving the B3LYP functional.[124−128] When comparing the computed values for CC_1 and its analogue in all of the 25 structural instances, the agreement is excellent. We have observed 1.489 Å for B3LYP, 1.485 Å for B3PW91, and 1.483 Å for PBE1PBE whereas the structural average is 1.49 Å with a standard deviation of 0.02 Å.

Also presented in Table 1 and Supporting Information, Table S1 are energetic and structural information calculated for the more sterically hindered ground state species **DA2**, **DA3**, and **DA3′**. Again there is excellent agreement in the prediction of θ_1, θ_2, and C−C bond distances across the different hybrid functionals. Again with respect to the Ru−N bond distances the B3PW91 and PBE1PBE functional models predict values in close agreement, and these are slightly shorter than those predicted by the B3LYP functional. With respect to the series of molecules and the dihedral angle that is critical to our conformational model, we observe θ_1 increasing (as expected) from 35 ± 1° for **DA1** to 50 ± 1° for **DA2** to 86 ± 1° and 88 ± 4° for **DA3** and **DA3′**, respectively, with these numbers representing an average $\pm 2\sigma$ of all the hybrid functional results. With the trend of increasing θ_1 across the series of increasing steric bulk on the aryl moiety we also observe an increase in CC_1 from 1.486 ± 0.006 Å for **DA1** to 1.491 ± 0.007 Å for **DA2** to 1.499 ± 0.004 Å and 1.501 ± 0.008 for **DA3** and **DA3′**, respectively, while CC_2, CC_3, and CC_4 remain very close to identical (changes are ≤0.003 Å) within each functional across the series of

(114) Beley, M.; Collin, J. P.; Louis, R.; Metz, B.; Sauvage, J. P. *J. Am. Chem. Soc.* **1991**, *113*, 8521–8522.
(115) Whittle, B.; Batten, S. R.; Jeffery, J. C.; Rees, L. H.; Ward, M. D. *J. Am. Chem. Soc.* **1996**, 4249–4255.
(116) Collin, J. P.; Kayhanian, R.; Sauvage, J. P.; Calogero, G.; Barigelletti, F.; DeCian, A.; Fischer, J. *Chem. Commun.* **1997**, 775–776.
(117) Chamchoumis, C. M.; Potvin, P. G. *J. Chem. Soc., Dalton Trans.* **1999**, 1373–1374.
(118) Mikel, C.; Potvin, P. G. *Inorg. Chim. Acta* **2001**, *325*, 1–8.
(119) Hartshorn, R. M.; Zibaseresht, R. *Arkivoc* **2006**, 104–126.
(120) Kan, J.; Zhang, L. Y.; Gao, L. B.; Shi, L. X.; Chen, Z. N. *Acta Crystallogr., Sect. E: Struct. Rep. Online* **2006**, *62*, M2255–M2256.
(121) Yoshikawa, N.; Yamabe, S.; Kanehisa, N.; Kai, Y.; Takashima, H.; Tsukahara, K. *Inorg. Chim. Acta* **2006**, *359*, 4585–4593.
(122) Yang, H. *Chem. J. Chin. Univ.* **2007**, *28*, 872.
(123) Brock, C. P.; Minton, R. P. *J. Am. Chem. Soc.* **1989**, *111*, 4586–4593.
(124) Zheng, K. C.; Wang, J. P.; Peng, W. L.; Liu, X. W.; Yun, F. C. *J. Mol. Struc. Theochem* **2002**, *582*, 1–9.
(125) Kato, M.; Takayanagi, T.; Fujihara, T.; Nagasawa, A. *Inorg. Chim. Acta* **2009**, *362*, 1199–1203.
(126) Stoyanov, S. R.; Villegas, J. M.; Rillema, D. P. *Inorg. Chem.* **2002**, *41*, 2941–2945.
(127) Borg, O. A.; Godinho, S.; Lundqvist, M. J.; Lunell, S.; Persson, P. *J. Phys. Chem. A* **2008**, *112*, 4470–4476.
(128) Alary, F.; Boggio-Pasqua, M.; Heully, J. L.; Marsden, C. J.; Vicendo, P. *Inorg. Chem.* **2008**, *47*, 5259–5266.

molecules. Presumably the increase in CC_1 tracks the sequential drop in π-system delocalization (resulting from back-bonding from the metal into the ligand-based π^* system) that is permitted in the ligands within the ground states of these complexes as steric repulsions are increased. The dihedral angle between pyridinium moieties in the acceptor fragment is insensitive to functional *and* species. The angle $\theta_2 \sim 40°$ is, like neutral biphenyl, dictated by the opposing interplay between π-delocalization electronic effects and repulsive steric interactions between hydrogen atoms ortho to the inter-ring C−C bond. The fact that θ_2 is insensitive to the species **DA1**, **DA2**, **DA3**, or **DA3′** reflects the relative electronic isolation of the acceptor moiety with respect to the donor metal-complex fragment. This is the expected result based the observation that visible absorption spectra are nearly identical between D and DA in systems related to **DA1**.[50] Although it is not a proof of electronic isolation between Donor and Acceptor, it is noted here that the HOMO Kohn−Sham molecular orbitals for **DA1**, **DA2**, **DA3**, and **DA3′** are largely metal based as shown in Supporting Information, Figure S1.

Regarding **DA2**, **DA3**, and **DA3′**, available computational and structural data for comparison with our results are somewhat limited. There are, to our knowledge, no reported computational results for Ru^{II} or Os^{II} coordination complexes with structurally similar bidentate or tridentate ligands. A crystal structure has been reported for the free ligand 4,4′-di-*o*-tolyl-2,2′-bipyridine[60] which is structurally similar to the active ligand in **DA2**. In this structure the measured $\theta_1 = 51.05°$ and $CC_1 = 1.488$ Å both of which are in excellent agreement with our computational results for all of the functionals. Structures for two different salts of a Pt^{II} species having a 4′-*o*-tolyl-terpyridine ligand have been reported. In these, θ_1 is larger than our prediction and varies from 65.2°−69.9° depending on counterion.[129]

For comparison with **DA3** and **DA3′**, a crystal structure has been reported for the free ligand 4,4′-dimesityl-2,2′-bipyridine (dmesb).[60] Here, $\theta_1 = 89.14°$, in close agreement with our results while the value for CC_1 (1.485 Å) is ∼0.015 Å shorter than our result. A structure has also been reported for $[Ru(dmesb)_3](PF_6)_2$. In this crystal a significant distribution of θ_1 (and CC_1: $1.49 \pm 0.02(2\sigma)$ Å) is observed such that McCusker and co-workers have reported an average over six dihedral angles in the complex of $\theta_1 = 70 \pm 10°$. These authors suggest the wide distribution of θ_1 and different orientations of the mesityl substituents relative to the three bipyridine planes may highlight soft torsional potentials through the perpendicular geometry ($\theta_1 = 90°$) and the role of crystal packing forces.[58]

At this stage, with the caveat that we cannot calculate the effects of intramolecular forces in crystals, there is a balance between excellent and reasonable agreement in our predictions of geometry for **DA1**, **DA2**, **DA3**, and **DA3′** and known structural data involving similar ligand motifs. This combined with good to excellent agreement in geometrical parameters across functionals and with other computational values in the literature suggests that geometries obtained using the functional models listed in Tables 1 and Supporting Information, Table S1 have sufficient accuracy to serve as models for the structural modifications that take place during the ET process in our systems.

^{3}MLCT Geometries. We are interested in understanding geometric and electronic changes that take place as our systems evolve from a Franck−Condon state with the geometry of the ground state to the lowest-energy excited state of the donor fragment (see Scheme 1). This latter state should then serve as the precursor to the ET photochemistry itself. The chromophoric excited-state donor is structurally and electronically very similar to $[Ru(dmb)_3]^{2+}$ and its well-characterized parent $[Ru(bpy)_3]^{2+}$, both of which form the ^{3}MLCT on an ultrafast time scale (∼100 fs)[130−133] following visible excitation in room-temperature solutions. In our systems, aryl ring rotation in the asymmetric ligand concomitant with electronic delocalization is expected on a ∼2 ps time scale.[63,134] The defining character of this observation is a time-dependent rise in a transient absorption signal for the MLCT photoexcited compound that occurs in a spectral region that is characteristic of a ligand-based radical anion that is delocalized over the bipyridine and the aryl substituent. Such a rise is not observed in compounds such as $[Ru(dmb)_3]^{2+}$ which do not have aryllated ligands.[63,134] As recently measured in similar systems by Browne, McGarvey, and co-workers, full vibrational thermalization in the ^{3}MLCT is expected on a ∼ 20 ps time scale.[135] Because initial events after photoexcitation in our systems are faster than the ET event itself (for **DA1**, $\tau_{ET} = 36$ ps in 298 K ACN)[50,136] computations illuminating the structure of the ^{3}MLCT state in our systems should model the excited-state precursor to ET. There is of course a significant caveat. With the SCF methods employed here, we cannot impose boundary conditions on the "charge-transferred" electron in systems like **DA1**, **DA2**, **DA3**, or **DA3′** in order to prevent the formation and geometry optimization of the lower energy ET states D^+-A^-. Rather, we need structural models whose lowest energy triplet state is MLCT in nature, and we utilize structures related to the **DA** species discussed above but with no electroactive methyl viologen moiety. This computational strategy has an important advantage. Because the lowest energy excited state is a triplet (the ^{3}MLCT) a simple open-shell geometry optimization gives us insight into excited-state structure. Others have also exploited lowest-energy triplet calculations of Ru species to explore states prepared in systems following photoexcitation.[80,90,113,127,128,137−139] It is noted

(129) Field, J. S.; Haines, R. J.; McMillin, D. R.; Summerton, G. C. *J. Chem. Soc., Dalton Trans.* **2002**, 1369–1376.

(130) Damrauer, N. H.; Cerullo, G.; Yeh, A.; Boussie, T. R.; Shank, C. V.; McCusker, J. K. *Science* **1997**, *275*, 54–57.

(131) Bhasikuttan, A. C.; Suzuki, M.; Nakashima, S.; Okada, T. *J. Am. Chem. Soc.* **2002**, *124*, 8398–8405.

(132) Yoon, S.; Kukura, P.; Stuart, C. M.; Mathies, R. A. *Mol. Phys.* **2006**, *104*, 1275–1282.

(133) Yeh, A.; Shank, C. V.; McCusker, J. K. *Science* **2000**, *289*, 935–938.

(134) McCusker, J. K. *Acc. Chem. Res.* **2003**, *36*, 876–887.

(135) Henry, W.; Coates, C. G.; Brady, C.; Ronayne, K. L.; Matousek, P.; Towrie, M.; Botchway, S. W.; Parker, A. W.; Vos, J. G.; Browne, W. R.; McGarvey, J. J. *J. Phys. Chem. A* **2008**, *112*, 4537–4544.

(136) Meylemans, H. A.; Hewitt, J. T.; Damrauer, N. H., in preparation **2009**.

(137) Batista, E. R.; Martin, R. L. *J. Phys. Chem. A* **2005**, *109*, 3128–3133.

(138) Charlot, M. F.; Pellegrin, Y.; Quaranta, A.; Leibl, W.; Aukauloo, A. *Chem.—Eur. J.* **2006**, *12*, 796–812.

(139) Alary, F.; Heully, J. L.; Bijeire, L.; Vicendo, P. *Inorg. Chem.* **2007**, *46*, 3154–3165.

Table 2. Energy and Structural Properties of the Lowest Energy Triplet for $[Ru(dmb)_2(4\text{-}p\text{-tolyl-}2,2'\text{-bipyridine})]^{2+}$ (**D1***), $[Ru(dmb)_2(4\text{-}(2,6\text{-dimethylphenyl})\text{-}2,2'\text{-bipyridine})]^{2+}$ (**D2***), $[Ru(dmb)_2(4\text{-mesityl-}2,2'\text{-bipyridine})]^{2+}$ (**D3***), and $[Ru(tmb)_2(4\text{-mesityl-}2,2'\text{-bipyridine})]^{2+}$ (**D3′***) Optimized in the Gas Phase[a,b]

method B3LYP	**D1*** (L = dmb)	**D2*** (L = dmb)	**D3*** (L = dmb)	**D3′*** (L = tmb)
energy (hartree)	−2006.8796	−2046.1826	−2085.4849	−2242.7317
$\langle S^2 \rangle$	2.0193	2.0176	2.0060	2.0135
θ_1 (av)	21.3°	34.9°	54.8°	55.9°
CC_1	1.460 Å	1.466 Å	1.483 Å	1.482 Å
CC_2	1.426 Å	1.425 Å	1.451 Å	1.420 Å
CC_3	1.474 Å	1.474 Å	1.449 Å	1.471 Å
RuN_1	2.016 Å	2.018 Å	2.066 Å	2.031 Å
RuN_2	2.093 Å	2.092 Å	2.101 Å	2.084 Å

[a] For all calculations the basis set for the Ru was LANL2DZ with an ECP and 631-G for the H, N, C atoms. [b] See Supporting Information, Table S2 for comparative results from calculations run using the B3LYP, B3PW91, and PBE1PBE functionals.

that the density of states in the triplet manifold is significantly higher than for the ground state singlet of our **D** models,[139−142] and our results will not be sensitive to any structural effects that might be induced by a Boltzmann distribution in multiple states.

As described in the Introduction, there are several computational studies in the literature that address excited-state electronic delocalization phenomena in aryl-substituted polypyridyl ligands of Ru^{II} or Os^{II}. In most of these, a geometry optimized doublet radical anion of a ligand species[60,75] or a doublet reduced metal complex[43,76,138,143] serves as a model of the MLCT state. The alternative is to consider the ground triplet state if it is MLCT in nature. Laine and Adamo have done this for Os^{II} species with 4′-aryl-substituted terpyridine ligands[43] and here we do it for the first time with Ru^{II} species having 4-aryl-substituted bipyridine ligands. It is our intuition that computations which preserve the close proximity of a formal Ru^{III} center to the charge-transferred electron, as is the case in a ^{3}MLCT state but not in a doublet radical anion calculation, should better reflect the electronic and nuclear consequences of excited state electron delocalization. Tables 2 and Supporting Information, Table S2 present energetic and structural information calculated for the lowest energy triplet state of donor species as gas-phase molecules. These calculations are referred to as **D1***, **D2***, **D3***, and **D3′*** because the lowest energy ^{3}MLCT in these systems is a common spectroscopic excited state.

We observe a slightly larger deviation in θ_1 for **D1*** as the functional is changed (3.2°) as compared to **DA1** (1.2°). However, the ^{3}MLCT has a soft potential energy surface with respect to θ_1 (vide infra), and we do not consider this result to be significant. In the cases of **D2***, **D3***, and **D3′***, the dihedral angle θ_1 deviates with functional by 1.7°, 2.3°, and 3.9°, respectively. Regarding **D1***, **D2***, **and D3′***, there is very little variation in C−C bond lengths as the density functional is changed as was seen for each of the **DA** species. Again, Ru−N distances for B3PW91 and PBE1PBE are close to each other and slightly shorter than B3LYP. This is irrespective of whether the bond length changes significantly in the dynamic model (see Scheme 1) as is the case for RuN_1 but not for RuN_2. The species **D3*** is somewhat more complex. Here there is excellent agreement in C−C bond lengths between B3LYP and B3PW91 but these deviate (especially CC_3) from that seen with PBE1PBE. This can be explained by changes in the spin density distribution in these triplet states as discussed below.

The MLCT nature of these lowest energy triplets can be assessed by visualization of the total spin density as shown in Figure 1 for **D1***, **D2***, **D3***, and **D3′***. The first two of these, **D1*** and **D2*** show excess α-spin (visualized by the blue regions) partitioned mainly between the Ru center and the aryl-substituted bipyridine ligand; that is, MLCT largely localized to the asymmetric aryl-substituted bipyridine ligand of interest. In the spin density distribution for **D3***, MLCT is still observed but now the charge transferred electron appears delocalized over all three ligands (favoring dmb2 and the asymmetric aryl-substituted bipyridine (see also Table 3 below)). As alluded to, differences in spin density suggest an explanation for anomalies in geometrical properties for **D3*** as a function of DFT functional. Supporting Information, Figure S2 indicates that the total spin density for **D3*** calculated with B3LYP and B3PW91 are very similar, each showing charge transfer to all three ligands, while spin density for the PBE1PBE calculation shows charge transfer almost exclusively to dmb2. This is why CC_3 is shorter in this calculation (vide supra).

The qualitative differences in spin density for **D3*** compared to either **D1*** or **D2*** suggests that the additional methylation of the aryl substituent, that is, going from a 2,4-dimethylphenyl substituent to a mesityl substituent, has a sufficient energetic perturbation such that the dmb moieties are no longer "high energy" ancillary ligands. To test this idea we compare total spin densities for the lowest energy triplet (^{3}MLCT) when the bidentate ligands (L) are varied by addition of electron donating methyl groups. Total spin density for **D3′*** (L = tmb) is shown in Figure 1 alongside that of **D3*** (L = dmb). Moving from the lower energy (more easily reduced) dmb ligand to the higher energy tmb ligand, the amount of spin density located on the asymmetric mesityl-bpy ligand undergoes a marked increase to the point where **D3′*** resembles both **D1*** and **D2*** in its directional MLCT quality. Because of these observations many of the comparisons made in subsequent portions of this manuscript will involve **D3′*** (and related **DA3′** and ^{3}**DA3′**) rather than **D3***.

To support the assignment of ^{3}MLCT in these calculations of **D*** we have also considered the total energy of **D1*** relative to **D1** using the B3LYP functional. Respectively, these are $E_{\mathbf{D1}^*} = -2006.8796$ hartree and $E_{\mathbf{D1}} = -2006.9592$ hartree such that the triplet is 2.17 eV higher in energy than the ground state. This result is in remarkably good agreement with the free energy difference of 2.11 eV between ^{3}MLCT and ^{1}GS measured for these systems in room temperature acetonitrile.[50,136] While

(140) Kober, E. M.; Meyer, T. J. *Inorg. Chem.* **1984**, *23*, 3877–3886.
(141) Lumpkin, R. S.; Kober, E. M.; Worl, L. A.; Murtaza, Z.; Meyer, T. J. *J. Phys. Chem.* **1990**, *94*, 239–243.
(142) Daul, C.; Baerends, E. J.; Vernooijs, P. *Inorg. Chem.* **1994**, *33*, 3538–3543.
(143) Charlot, M. F.; Aukauloo, A. *J. Phys. Chem. A* **2007**, *111*, 11661–11672.

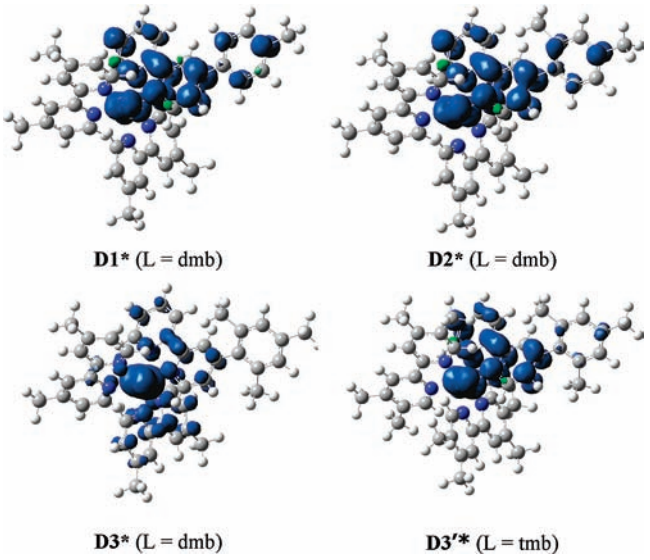

Figure 1. Spin density distributions (contour value = 0.0025) for the optimized ^{3}MLCT state using the B3LYP functional. Excess α-spin is visualized by blue regions whereas excess β-spin is green.

these are gas-phase calculations and the measurements are in solution, the energetic agreement occurs because solvation is not treated for either the singlet ground state or the lowest energy triplet and the significant error in energy for either calculation is largely canceled in the determination of an energy difference. Similar results involving the cancellation of solvation errors have been observed by others.[76,80,126,138]

The geometric changes, and by inference electronic changes, that take place as our systems evolve from a Franck−Condon state to the lowest-energy excited state of the donor fragment (see Scheme 1) can be assessed by comparing key geometrical parameters for **D1*** versus **DA1**, **D2*** versus **DA2**, **D3*** versus **DA3**, and **D3′*** versus **DA3′** from Tables 1 and 2, and Supporting Information, Tables S1 and S2. For our purposes the most important feature is the planarization of the bridge for each of these species referred to as $\Delta\theta_1$ (defined as $\theta_{1\mathbf{D}^*} - \theta_{1\mathbf{DA}}$). For the comparison between **D1*** and **DA1**, $\Delta\theta_1 = -13.3°$ (B3LYP), $-12.6°$ (B3PW91), and $-11.1°$ (PBE1PBE). For **D2*** and **DA2**, $\Delta\theta_1 = -15.0°$ (B3LYP), $-14.6°$ (B3PW91), and $-12.8°$ (PBE1PBE). For **D3*** and **DA3**, $\Delta\theta_1 = -30.7°$ (B3LYP), $-29.5°$ (B3PW91), and $-30.8°$ (PBE1PBE). Finally, for **D3′*** and **DA3′**, $\Delta\theta_1$ is quite similarly $= -29.6°$ (B3LYP), 31.6° (B3PW91), and 29° (PBE1PBE). In all cases large amplitude motions are observed. It is interesting to us that these motions are largest for the cases involving the most steric bulk, that is, **D3*** versus **DA3** and **D3′*** versus **DA3′**. As discussed later this may have important consequences for control of back ET rates. Concomitant with ring rotation there are also significant bond length changes in these systems upon relaxation from the Franck−Condon state. Figure 2 summarizes the effects in the aryl-substituted ligand and its metal coordination by showing which bonds contract (red) and which extend (green) in the difference between ^{3}MLCT (**D***) and ground state (**DA**). The thickness of the colored lines is proportional to the observed change. In all cases CC_1 contracts (the C−C bond between bipyridine and the aryl substituent) with the amount (−0.029 Å)

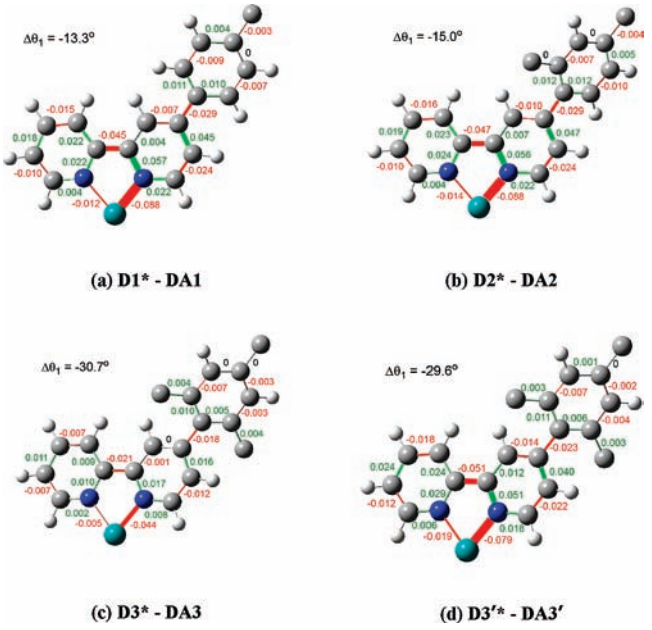

Figure 2. Summary of bond length changes (in Å) on the aryl-substituted ligand when going from the ground state singlet (DA) to the ^{3}MLCT (D*) using the B3LYP functional. Bond length extensions are green and contractions are red. The line thickness is proportional to the observed change.

being larger for the first two cases (**a**) and (**b**) involving the least steric encumbrance and intermediate steric encumbrance, respectively. Bond length changes within the bipyridine fragment are similar for cases (**a**), (**b**), and (**d**). The lack of significant changes for (**c**) is consistent with the more delocalized spin density with respect to all polypyridyl ligands (Figure 1).

From these it is our conclusion that no simple representation akin to a resonance picture emerges for the π-system, which includes M-L bonding, the fused pyridyl heterocycles of bipyridine, and one aryl substituent that must accommodate the additional charge transferred during MLCT. Nonetheless contraction of CC_1 by a significant amount and bond length changes in the aryl substituents themselves are good indicators that the transferred electron is delocalizing in a larger π-system that includes these rings. This supports our intuition that ring rotation involving changes to θ_1 occur to accommodate extended excited-state delocalization. One observation that we find surprising concerns (**c**) and (**d**). Despite large changes in spin density toward the aryl-substituted bipyridine ligand on going from **D3*** to **D3′*** we do not see a larger $-\Delta\theta_1$ nor substantial differences in the bond length changes of the mesityl substituent. Additional theoretical investigation to better understand why this is the case may be warranted if compounds of this nature show promising control of ET rates.

The geometric changes we are observing are smaller than what is observed in the original computational model that used 4-phenylpyridine, 4-(*o*-Tolyl)pyridine, and 4-(2,6-dimethylphenyl)pyridine and their respective reduced forms to explore excited-state delocalization following MLCT.[60] There, using (4-phenylpyridine)$^-$ versus 4-phenylpyridine as an example, the geometrical analogue of $\Delta\theta_1$ is $\sim -45°$. We interpret the smaller changes in systems here to be a consequence of the larger and electronically more complex multi-ring structures in

Table 3. Spin Population for Each Subunit in the Triplet Optimizations Calculated with a Mulliken Partition Scheme

subunit	D1*	D2*	D3*	D3′*	^{3}DA1	^{3}DA2	^{3}DA3	^{3}DA3′
Ru	0.669602	0.680788	0.944820	0.795276	0.965165	0.969623	0.979127	0.976074
L1	−0.002989	−0.000409	0.138489	−0.008121	0.001790	0.002071	0.005072	0.010139
L2	0.009763	0.005557	0.450657	0.003010	0.008266	0.007186	0.002253	0.009875
bpy	1.11207	1.110597	0.418351	1.114354	0.338260	0.344155	0.388099	0.317620
bridge	0.204795	0.190316	0.034464	0.092951	0.028781	0.017894	0.000008	0.002834
spacer	0.005047	0.004723	0.001021	0.002531	−0.003234	−0.002723	−0.002066	−0.002343
acceptor					0.660947	0.669772	0.622131	0.685793

the actual metal complexes where the charge-transferred electron is partitioned. Note that in all cases in Figure 2, there are significant geometrical changes in RuN_1 and CC_2 (larger than for CC_1), both of which are absent in the original 4-phenylpyridine model. With additional bonding to participate in the delocalization it appears that an energetic balance is being struck between the stabilization gained through ring rotation and contraction of CC_1 and the destabilization resulting from increased steric repulsions.

Some caution should be exercised to avoid over-interpreting the differences we see here in $\Delta\theta_1$ compared to other computational models (e.g., reference 60) and how these might manifest in experimental systems that are in solvent environments. Using the B3LYP functional (and the same basis set as has been discussed) we have calculated a torsional potential curve for **D1*** by fixing the geometrical parameter θ_1 while allowing other parameters to fully relax (Figure 3). These calculations suggest there is little energetic consequence to rotation through $\theta_1 = 0°$ where the barrier is 0.39 kcal/mol (0.0169 eV); that is, less than the room temperature value for kT (298 K = 0.59 kcal/mol (0.0257 eV)). While such a barrier height is below the trusted accuracy of DFT methods, we might presume that a distribution of dihedral angles (including ones near $\theta_1 = 0°$) are sampled in the ^{3}MLCT of **DA** systems prior to ET.

For each of the systems **D1***, **D2***, **D3***, and **D3′*** we have considered how much energy is released in the formation of the optimized triplet geometry from a triplet with the nuclear geometry of the Franck−Condon state. This is done by comparing energies of the geometry optimized species with single point energies calculated using relevant geometrical parameters from optimized structures of **DA1**, **DA2**, **DA3**, and **DA3′**, respectively (see the Computational Methods for details regarding how the terminal methyl group that is absent in **DA1**, **DA2**, **DA3**, and **DA3′** is handled). The $\Delta E'$ from this treatment has the following definition, $\Delta E' = E_{\text{TripletOptimized}} - E_{\text{TripletFranck−Condon Single Point}}$. In the three dmb-containing complexes $\Delta E' = -7$ kcal/mol (−0.30 eV) while for the tmb-containing species, $\Delta E' = -9$ kcal/mol (−0.39 eV). In this latter case the more electron rich ancillary tmb ligands are better able to stabilize the formal Ru^{III} center produced via MLCT thereby leading to shorter Ru−N bond distances and more energy released compared to the dmb-containing complexes.

Using **D1*** and the potential curve of Figure 3 we can ask how much of −7 kcal/mol (−0.30 eV) in reorganization energy from the Franck−Condon geometry is due to torsion as opposed to, for example, bond length changes (again, all bond lengths are allowed to relax at each point on the curve). In Figure 3 the energy difference between

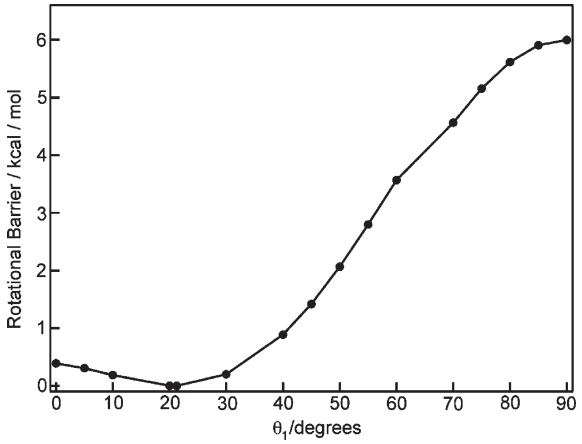

Figure 3. Potential surface for rotation about θ_1 in **D1*** (B3LYP functional). For these calculations the dihedral θ_1 was locked, and the rest of the structure was allowed to optimize. The barrier height through 0° is 0.39 kcal/mol (0.0169 eV) and through 90° is 6.0 kcal/mol (0.260 eV).

$\theta_1 = 34.6°$ (the value at the ground state **DA1** geometry (B3LYP)) and $\theta_1 = 21.3°$ (the minimum) is ∼0.5 kcal/mol (0.022 eV) suggesting that 7% of −7 kcal/mol (−0.30 eV) is due to torsion alone. This value is substantially less than the low-frequency torsional reorganization energy of 0.13 eV (3 kcal/mol) reported by Miller and co-workers for the oxidation of biphenyl anion.[144] However, in their study, torsion is complete, that is, the change in the inter-ring dihedral angle is ∼45°. Further, and more importantly, the additional charge (creating the anion) only occupies a two-ring π-system. In our case additional charge supplied by the MLCT event occupies a larger and more complex π-system which includes metal−ligand bonding (vide supra) such that reorganization requiring low frequency torsion plays a smaller role.

As a final comment on excited state delocalization in these **D*** systems, we report the spin population calculated with the Mulliken partition scheme as a function of subunit (see Scheme 2 for definitions) in Table 3 (this includes ^{3}**DA** systems, vide infra). The sum of numbers in each column is ≅ 2. This reflects the fact that these are triplets and that the effects of spin polarization in these molecules (as predicted by these calculations) are minor (note that in all plots of spin density in this paper there is very little excess β-spin (green) observed).[145] As seen in Figure 1, spin density for **D3*** is delocalized over all polypyridyl ligands which is reflected in significant spin population for L1, L2, and bpy. For the systems **D1***,

(144) Miller, J. R.; Pavlatos, B.; Bal, R.; Closs, G. L. *J. Phys. Chem.* **1995**, *99*, 6923–6925.
(145) Ruiz, E.; Cirera, J.; Alvarez, S. *Coord. Chem. Rev.* **2005**, *249*, 2649–2660.

D2*, and **D3′*** spin density on ancillary ligands is small and a more reliable comparison might be made as to how much resides on the bridge, signaling delocalization. Here we see evidence that ~20%, 19%, and 9% of the spin of an electron resides there for **D1***, **D2***, and **D3′***, respectively. It is noteworthy that changing the dihedral angle θ_1 from ~21° in **D1*** (B3LYP) to ~35° in **D2*** has little influence on the spin density of the bridge, suggesting this degree of steric bulk may not play a large role hindering forward ET rates. Experiments that are currently underway support this finding. By addition of more steric bulk (i.e., in **D3′***) we do observe decreased spin density on the bridge but emphasize that it, and therefore extended excited state delocalization of the MLCT electron, is not eliminated.

$^3D^+A^-$ Geometries. In previous and current work we have measured the rate of formation of $^3D^+-A^-$ in room temperature acetonitrile for three close structural analogues where the two ancillary ligands (L) are varied to include L = bpy, dmb (i.e., **DA1**), and tmb.[50,136] Across the series of molecules the measured ET rate constants are very similar with $k_{ET} = 2.6 \times 10^{10}$ s^{-1} (L = bpy), $k_{ET} = 2.8 \times 10^{10}$ s^{-1} (L = dmb), and $k_{ET} = 2.8 \times 10^{10}$ s^{-1} (L = tmb). In our interpretation of these results, the narrow distribution of rate constants even as ΔG°_{ET} is varied through 100 meV, is a consequence of excited-state electronic delocalization in D*−A and its effect on reorganization energies. On the other hand, back ET rate constants ($D^+-A^- \rightarrow D-A$) vary substantially across this series largely reflecting where these systems sit energetically in the Marcus inverted region ($k_{BET} = 0.6 \times 10^{10}$ s^{-1} (L = bpy), $k_{BET} = 1.1 \times 10^{10}$ s^{-1} (L = dmb), and $k_{BET} = 1.4 \times 10^{10}$ s^{-1} (L = tmb). In these data, comparative information is lacking that might confirm or refute the ligand motion switching in step (iv) of the dynamic model proposed in Scheme 1. We therefore turn to computational models in this section to explore these ideas.

Table 4 and Supporting Information, Table S3 present energetic and structural information for our calculations of the lowest energy triplet in the DA systems, referred to as **^{3}DA1**, **^{3}DA2**, **^{3}DA3**, and **^{3}DA3′**. For both **^{3}DA1** and **^{3}DA2** the observed deviation in θ_1 as the functional is changed is small (≤1.5°). It is slightly larger for the **^{3}DA3** and **^{3}DA3′** species where a deviation of 4.7° and 3.7°, respectively, is seen between the PBE1PBE and B3PW91 functionals. However, we do not place much significance on this deviation. It will be shown below that there is no significant spin density on the bridge for these triplets, and one might infer that energy differences within a 4.7° dihedral angle θ_1 variation are insignificant. Again, there is little variation in C−C bond lengths as the density functional is changed as was seen for each of the **DA** species and for the **D1***, **D2***, and **D3′*** systems. The largest variation occurs for CC_1 between PBE1PBE and B3LYP with the former predicting a bond length 0.009 Å shorter than the latter. As seen for both **DA** and **D*** calculations (vide supra), Ru−N distances for B3PW91 and PBE1PBE are close to each other and slightly shorter than B3LYP.

Table 4 and Supporting Information, Table S3 also present the calculated energy of **^{3}DA1**, **^{3}DA2**, **^{3}DA3**, and **^{3}DA3′** relative to their respective singlet ground states **DA1**, **DA2**, **DA3**, and **DA3′**; that is, $\Delta E = E_{3DA} - E_{DA}$. For all four species there is excellent agreement in the calculated ΔE as the functional is varied. We observe $\Delta E_{DA1} = 1.45 \pm 0.02$ eV, $\Delta E_{DA2} = 1.49 \pm 0.03$ eV, $\Delta E_{DA3} = 1.55 \pm 0.03$ eV, and $\Delta E_{DA3'} = 1.37 \pm 0.05$ eV where the value and error represent the average and two times the standard deviation, respectively, as the functional is altered. In terms of experimental comparisons, ΔE is most closely related to $-\Delta G^\circ_{BET} = \Delta G^\circ_{IP}$ where ΔG°_{BET} is the free energy available for back ET and ΔG°_{IP} is the free energy needed to generate the ion-pair state. For **DA1** in acetonitrile solvent we have measured $-\Delta G^\circ_{BET} = 1.53$ eV. Again, the gas-phase calculations ($\Delta E_{DA1} = 1.45 \pm 0.02$ eV) show quite reasonable agreement indicating a fortuitous cancellation of errors when solvation is ignored for both the lowest energy singlet and the lowest energy triplet states. We find ΔE for **^{3}DA3′** (where L = tmb) is smaller than for each of the other species (where L = dmb) which is an expected result. The more electron donating quality of the tmb ligand versus the dmb ligand should make the oxidation potential of the donor portion of the molecule easier, thereby driving down the energy released in the formation of the ion pair state. We (and many others) see this in experimental systems by varying ancillary ligands.[50,146] For these same reasons the trend (although subtle) wherein ΔE increases with additional steric bulk on the aryl substituent from ΔE = 1.45 eV (**^{3}DA1**) to 1.49 eV (**^{3}DA2**) to 1.55 eV (**^{3}DA3**) is unexpected. This is the first indication that the singly occupied molecular orbital (SOMO) in these calculations is not isolated to the acceptor moiety. This is discussed more below.

In support of the ligand-based switching in step (**iv**) of the dynamic model proposed in Scheme 1, θ_1 in Table 4 for all species shows a larger optimized value than what is seen in Table 2 for the respective **D*** species. Whereas $\Delta\theta_1$ was defined previously as $\Delta\theta_1 = \theta_1(\mathbf{D^*}) - \theta_1(\mathbf{DA})$, here we define $\Delta\theta_1' = \theta_1(^3\mathbf{DA}) - \theta_1(\mathbf{D^*})$. Based on B3LYP values, $\Delta\theta_1' = +6.7°$ for **^{3}DA1**, $\Delta\theta_1' = +9°$ for **^{3}DA2**, $\Delta\theta_1' = +19°$ for **^{3}DA3**, and $\Delta\theta_1' = +25.4°$ for **^{3}DA3′**. Concomitant with this reverse ring rotation there are also significant bond length changes that occur including the lengthening of CC_1: (based on B3LYP values) $\Delta CC_1' = +0.019$ Å for **^{3}DA1**, **^{3}DA2**, and **^{3}DA3′**, with $\Delta CC_1' = +0.017$ Å for **^{3}DA3** being slightly shorter. On one hand these dihedral angle and bond length changes are supportive of the hypothesis put forth in Scheme 1 suggesting reverse motions may be useful for decreasing back ET rates. On the other hand the relative changes are less than expected and do not restore these key geometrical parameters such as θ_1 and CC_1 to their ground state values. For example, the value for θ_1 in **^{3}DA1** is $\theta_1 = 28°$ (B3LYP) or 6.6° shy of the ground state value (**DA1**) where θ_1 = 34.6° (see Table 1). This 6.6° is not an insignificant amount given that $\Delta\theta_1$ = 13.3° for this system (vide supra).

Total spin density calculated for these triplet systems offers insight into the origin of these observations. As shown in Figure 4, significant unpaired spin resides, as expected, on the ruthenium atom and the acceptor subunit. However, there is also an unexpected "pocket" of

(146) Juris, A.; Balzani, V.; Barigelletti, F.; Campagna, S.; Belser, P.; Von Zelewsky, A. *Coord. Chem. Rev.* **1988**, *84*, 85–277.

Table 4. Energy and Structural Properties of the Lowest Triplet State for $[Ru(dmb)_2(bpy\text{-}\phi\text{-}MV)]^{4+}$ (^{3}**DA1**), $[Ru(dmb)_2(bpy\text{-}o\text{-}tolyl\text{-}MV)]^{4+}$ (^{3}**DA2**), $[Ru(dmb)_2(bpy\text{-}2,6\text{-}Me_2\text{-}\phi\text{-}MV)]^{4+}$ (^{3}**DA3**), and $[Ru(tmb)_2(bpy\text{-}2,6\text{-}Me_2\text{-}\phi\text{-}MV)]^{4+}$ (^{3}**DA3′**) Optimized in the Gas Phase[a,b]

method B3LYP	^{3}DA1 (L = dmb)	^{3}DA2 (L = dmb)	^{3}DA3 (L = dmb)	^{3}DA3′ (L = tmb)
energy (hartree)	−2540.7628	−2580.0670	−2619.3726	−2776.6256
$\langle S^2 \rangle$	2.0081	2.0078	2.0072	2.0075
ΔE (eV)	1.450	1.500	1.555	1.380
θ_1 (av)	28.0°	43.9°	73.8°	81.3°
θ_2 (av)	14.8°	12.7°	15.8°	13.7°
CC_1	1.479 Å	1.485 Å	1.500 Å	1.501 Å
CC_2	1.457 Å	1.456 Å	1.452 Å	1.456 Å
CC_3	1.473 Å	1.474 Å	1.473 Å	1.469 Å
CC_4	1.456 Å	1.455 Å	1.457 Å	1.453 Å
RuN_1	2.092 Å	2.095 Å	2.101 Å	2.108 Å
RuN_2	2.106 Å	2.103 Å	2.098 Å	2.104 Å

[a] For all calculations the basis set for the Ru was LANL2DZ with an ECP and 631G for H, N, and C. [b] See Supporting Information, Table S3 for comparative results from calculations run using the B3LYP, B3PW91, and PBE1PBE functionals.

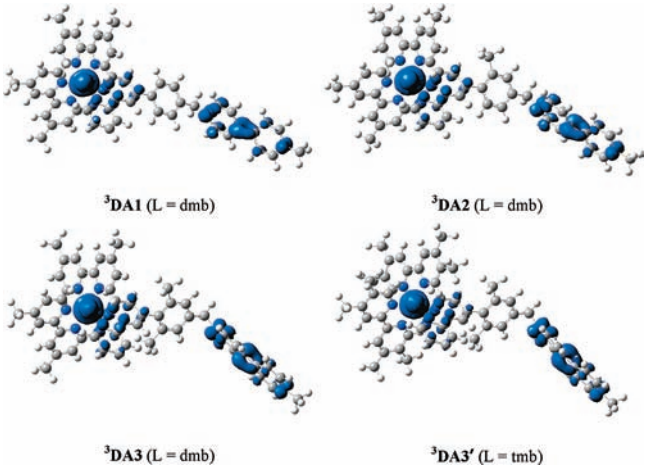

Figure 4. Spin density distributions (contour value = 0.0025) for the optimized lowest triplet state of the full donor−acceptor complex using the B3LYP functional. Excess α-spin is visualized by blue regions whereas excess β-spin is green (very little is seen).

unpaired spin that is found on the bipyridine fragment of the asymmetric aryl-substituted ligand in each of the species ^{3}**DA1**, ^{3}**DA2**, ^{3}**DA3**, and ^{3}**DA3′**.

Examination of the spin populations (Table 3) as a function of subunit shows this quantitatively. In each of these four systems the spin of an electron is shared approximately 1/3 on the bipyridine fragment to 2/3 on the acceptor unit. This is also the nature of the highest occupied Kohn−Sham molecular orbital in these systems as shown in Supporting Information, Figure S3. Evidently in these gas phase calculations, the lowest energy triplet is achieved by partitioning on to the central bipyridine a significant part of the electron density that we would normally expect to reside on the more easily reduced MV^{2+} acceptor moiety. It is assumed that a triplet of this nature is most stable because of Coulombic interaction of electron density residing on the bipyridine with the proximal Ru^{3+} center. However, this can only be achieved if the highest occupied molecular orbital (HOMO) provides an opportunity for electron delocalization throughout the bipyridine unit, aryl bridge, and on to the MV^{2+} acceptor moiety, and such a property would be assisted by a smaller dihedral angle θ_1 and a smaller CC_1 bond length.

The unusual or at least unexpected distribution of spin density outside of the acceptor moiety in the systems discussed above lead us to consider simple solvation models using the PCM continuum methodology parametrized for acetonitrile. With geometries of ^{3}**DA1**, ^{3}**DA2**, ^{3}**DA3**, and ^{3}**DA3′** fixed to the gas-phase values discussed in Table 4, the total spin density distributions shown in Figure 5 are now observed.

For each system we now see spin density of very close to one on the acceptor moiety (0.996 from the spin population calculated with a Mulliken partition scheme for ^{3}DA1) and on the metal center (0.961 from the spin population calculated with a Mulliken partition scheme for ^{3}DA1) suggesting that solvation of a complete charge on the acceptor makes a larger contribution to lowering the energy of the system than a Coulombic interaction between charge residing on the bipyridine fragment and the Ru^{3+} center. This modified spin density is in better agreement with expectations about the physical behavior of such systems based on redox chemistry.[50]

This result, combined with the hypothesis mentioned above that spin density which includes the bipyridine fragment might be responsible for reduced values of θ_1, lead us to consider geometry optimizations of the full system within an acetonitrile solvent continuum model. These are computationally intensive calculations that are difficult to converge so we only present results for ^{3}**DA1** and **DA1** geometry optimizations. We also wanted to compare structures of approximately the same size and with a similar cavity within the continuum model. The spin density for the ^{3}**DA1** geometry optimized with a PCM continuum (acetonitrile) model is shown in Figure 6. The main features at the acceptor and metal center are in agreement with the single point PCM calculations shown in Figure 5. Spin populations calculated with a Mulliken partition scheme indicate 49% of the excess α-spin on the metal and 50% on the acceptor moiety.

Energetic and geometrical parameters for the PCM continuum model optimized geometries are shown in Table 5 alongside information for **DA1** and ^{3}**DA1** that were also presented in Tables 1 and 4, respectively. The calculated ΔE = 1.5 eV between **DA1 PCM** and ^{3}**DA1 PCM** is in excellent agreement with experiment where 1.53 eV has been measured.[136] The most striking and satisfying result here is that θ_1 of the ^{3}**DA1 PCM** optimization is θ_1 = 32.9° compared with θ_1 = 28.0° without solvation (^{3}**DA1**). This suggests that all (if we refer to the **DA1 PCM** result) of the dihedral angle reverse switching, that is, step (**iv**) of Scheme 1, is achieved with the more experimentally relevant computational model (i.e., a model with solvation). Also of note is the significant large amplitude motions in the acceptor moiety with respect to the **DA1 PCM** ground state calculation characterized by an ∼ −36° change in θ_2 (essentially complete planarization in this two-ring system) and a −0.045 Å bond length change to CC_4.

This result of full reverse switching in the presence of polar solvation has important implications for ET control as it pertains to decreasing rate constants for back ET (k_{BET}). We presume that the electronic coupling between

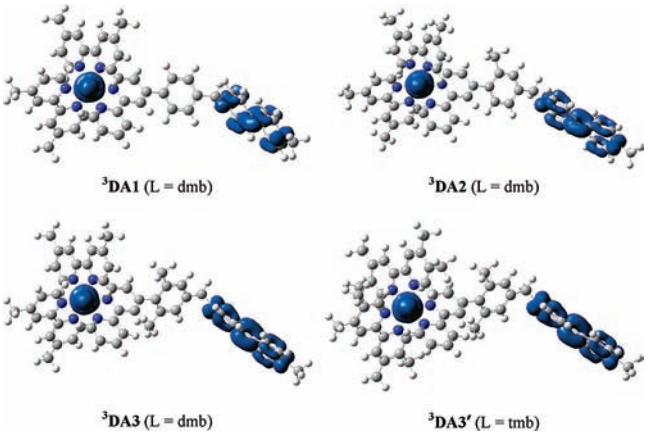

Figure 5. Spin density distributions (contour value = 0.0025) for single point calculations using the B3LYP functional and PCM parameterized for acetonitrile (the geometry is that of the optimized ^{3}DA using B3LYP). Excess α-spin is visualized by blue regions whereas excess β-spin is green (very little is seen).

donor and acceptor in these systems (H_{DA}), where the donor is the reduced methyl viologen and the acceptor is the oxidized metal center, is governed by superexchange[147] allowing us to invoke a modified form of the common McConnell expression approximating H_{DA}:

$$H_{DA} = \frac{V_{DB}V_{B'A}}{\Delta}\left(\frac{V_{BB'}}{\Delta'}\right) \quad (1)$$

In this expression, Δ reflects an energy difference between states localized on the donor (the reduced methyl viologen in this case) versus the aryl substituent of the bridge while Δ′ reflects an energy difference between states localized on donor versus the bipyridine fragment of the bridge. V_{DB}, $V_{B'A}$, and $V_{BB'}$ are electronic coupling strengths between donor and aryl-localized bridge states, bpy-localized bridge states and acceptor states, and between localized states in the separate π-systems (aryl and bpy) on the bridge, respectively. Use of superexchange is reasonable because the asymmetric aryl-substituted bipyridine moiety within **DA1** and model donor metal complexes **D1**, **D2**, **D3**, and **D3′** are more difficult to reduce than MV^{2+} by ~1 eV in acetonitrile[50,136] suggesting that reduction of the bridge (even including the covalently attached bpy) would be a high energy intermediate in an incoherent hopping mechanism. Superexchange has been shown to be highly sensitive to torsional angles θ that influence electronic coupling between conformationally active π-systems.[23−25,27,28,30,34,39,41,148] If we make the common assumption (based on the overlap between p-orbitals) that $V_{BB'} = V_{BB'}^{\circ}\cos(\theta_1)$, where $V_{BB'}^{\circ}$ refers to coupling between bridge π-systems (aryl and bpy) when $\theta_1 = 0°$, then the back ET rate constant for **DA1**, **DA2**, or **DA3** can be written as

$$k_{BET}(\theta_1) = \cos^2(\theta_1) \times k_{BET}^{\circ} \quad (2)$$

where k_{BET}° is a hypothetical rate constant if the dihedral angle $\theta_1 = 0°$. In writing down a common expression for **DA1**, **DA2**, and **DA3** the gross assumption is being made

(147) McConnell, H. *J. Chem. Phys.* **1961**, *35*, 508–515.
(148) Eng, M.; Albinsson, B. *Chem. Phys.* **2009**, *357*, 132–139.

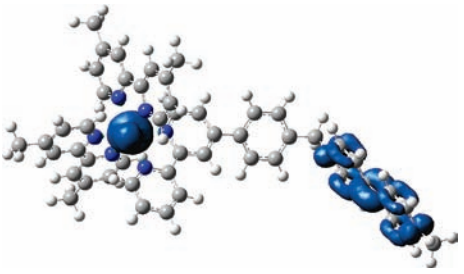

Figure 6. Spin density distribution (contour value = 0.0025) for the optimized lowest triplet state for the full donor−acceptor complex, ^{3}DA1, using the B3LYP functional and PCM parametrized for acetonitrile. Excess α-spin is visualized by blue regions whereas excess β-spin is green (very little is seen).

Table 5. Energy and Structural Properties for $[Ru(dmb)_2(bpy\text{-}\phi\text{-}MV)]^{4+}$ (DA1) and the Lowest Energy Triplet State of $[Ru(dmb)_2(bpy\text{-}\phi\text{-}MV)]^{4+}$ (^{3}DA1) Optimized in Both Gas Phase and within a PCM Model Parameterized for Acetonitrile[a]

method B3LYP	**DA1** gas phase	**^{3}DA1** gas phase	**DA1 PCM**	**^{3}DA1 PCM**
energy (hartree)	−2540.8162	−2540.7627	−2541.3826	−2541.3270
$\langle S^2\rangle$		2.0081		2.0088
ΔE (eV)		1.454		1.513
θ_1 (av)	34.6°	28.0°	32.1°	32.9°
θ_2 (av)	39.5°	14.8°	36.7°	0.2°
CC_1	1.489 Å	1.479 Å	1.481 Å	1.477 Å
CC_2	1.472 Å	1.457 Å	1.471 Å	1.469 Å
CC_3	1.474 Å	1.473 Å	1.473 Å	1.471 Å
CC_4	1.490 Å	1.456 Å	1.481 Å	1.436 Å
RuN_1	2.104 Å	2.092 Å	2.102 Å	2.094 Å
RuN_2	2.105 Å	2.106 Å	2.102 Å	2.102 Å

[a] For all calculations the Basis set for the Ru was LANL2DZ with an ECP and 631-G for the H, N, C atoms.

that each system is identical in reorganization energy, driving force, ET distance, donor-bridge coupling, bridge-acceptor coupling, etc., and that all that is changing is the torsional angle θ_1. Using the measured value for $k_{BET\mathbf{DA1}} = 1.08 \times 10^{10}\ s^{-1}$ in room temperature acetonitrile and values for θ_1 from the gas-phase ground state **DA** B3LYP calculations (Table 1),

$$k_{BET}(35°) = 1.08 \times 10^{10}\ s^{-1} = \cos^2(35°) \times k_{BET}^{\circ} \quad (3)$$

Solving for k_{BET}° and using it in the following two expressions allows us to predict k_{BET} and therefore τ_{BET} for both **DA2** and **DA3** (or **DA3′**).

$$k_{BET}(50°) = \cos^2(50°) \times k_{BET}^{\circ} \quad (4a)$$

$$k_{BET}(86°) = \cos^2(86°) \times k_{BET}^{\circ} \quad (4b)$$

These expressions suggest a single methyl substituent on the bridge, that is, **DA2**, will lead to a $\mathbf{D^+A^-}$ charge separation lifetime τ_{BET} of 150 ps compared to 93 ps measured for **DA1**. Recent measurements in our laboratory which will be reported shortly show $\tau_{BET} = 220$ ps (**DA2**) which is in reasonable agreement with this crude model.[136] A decrease in ET rates that is explained in a similar way has been observed by Indelli, Scandola, and co-workers for certain $Ru^{II}-Rh^{III}$ dyads.[45] The more interesting case is **DA3** (or **DA3′**) where two methyl substituents force a dihedral angle near 90° such that

$V_{BB'}$ is small. Here the crude model predicts $\tau_{BET} = 12.8$ ns, that is, a charge separated lifetime 139 times larger than that observed for **DA1**.[149] It is noted that there is experimental[30,39] and computational[24,51] evidence that electronic coupling for ET between π-systems can be related to $\cos^n(\theta_1)$ where $n > 1$ (and often $n = 2$). With a similar analysis to what is shown in eqs. 3,4a, and 4b, but now using $V_{BB} = V_{BB}^{\circ} \cos^2(\theta_1)$, τ_{BET} is predicted to be 250 ps for **DA2** (also in reasonable agreement with our recent measurement) and 1.8 μs for **DA3** (or **DA3′**). This latter quantity suggests a charge separated lifetime greater than 19000 times than that observed for **DA1**.

If the forward ET rate constant for **DA3** or **DA3′** can be kept reasonably large, such systems will be valuable molecular switches with a high quantum yield of charge separation and the capability of storing redox equivalents at moderate distances for a chemically significant amount of time. Fast forward ET in **DA3** or **DA3′** is a distinct possibility. The spin density predictions shown in the last section suggest electron density on the bridge from MLCT reaches 9% even when $\theta_1 = 55°$ (Table 3 for **DA3′**). This is an encouraging amount compared to the 20% and 19% calculated for **DA1** and **DA2**, respectively (vide supra). These are both systems for which forward ET is fast with τ_{ET} in room temperature acetonitrile measured to be 36 ps for **DA1** and 37 ps for **DA2**.[136]

Conclusions

In this paper we have applied DFT using three different hybrid HF/DFT functionals, B3LYP, B3PW91, and PBE1PBE, to explore conformational changes that follow charge transfer and ET steps in photoexcited Donor−Acceptor complexes being studied in our laboratory. In the ground electronic state of such systems, aryl substituents, which participate in the bridge between a chromophoric Ru^{II} metal complex and an electroactive methyl viologen moiety, assume a non-coplanar geometry relative to a bipyridine ligand of the metal center. This is the expected result based on comparisons with known species having aryl−aryl couplings. For the systems under consideration, **DA1** (L = dmb), **DA2** (L = dmb), **DA3** (L = dmb), and **DA3′** (L = tmb) the three different DFT functionals show optimized structures (gas-phase calculations) in close agreement with respect to the dihedral angle θ_1 defining the orientation of the aryl substituent and the bipyridine to which it is covalently bound. The least sterically encumbered **DA1** exhibits $\theta_1 = 35 \pm 1°$ for the three different functionals (error is two times the standard deviation) in good agreement with other DFT and X-ray structural reports in the literature for geometrically related metal complexes. For **DA2**, $\theta_1 = 50 \pm 1°$ and for the most sterically encumbered **DA3** and **DA3′** $\theta_1 = 86 \pm 1°$ and $\theta_1 = 88 \pm 3°$, respectively. Key C−C bond lengths show excellent agreement across DFT functionals and with X-ray structural data for related systems when it has been available.

The optimized geometries (again as a function of the DFT functional and again with gas-phase calculations) for the lowest energy triplet state of donor complexes **D1***, **D2***, **D3***, and **D3′*** were explored to model conformational changes that follow MLCT excitation in these systems. Each exhibits large amplitude torsional motions with inter-ring dihedral angles measured relative to respective ground state **DA** results of $\Delta\theta_1 = -12 \pm 2°, -14 \pm 2°, -30 \pm 1°, -30 \pm 3°$ for **D1***, **D2***, **D3***, and **D3′***, respectively. The total spin density in **D1***, **D2***, and **D3′*** supports the assignment that excited-state intraligand electronic delocalization drives conformational changes associated with $\Delta\theta_1$ as well as C−C bond length changes such as the reduction in CC_1 which is the bond distance between the aryl and bipyridine fragments. The conformational changes we are observing in these metal complexes following relaxation of the ^{3}MLCT are smaller than those seen in simple two-ring models which compare 4-aryl-pyridine species with their one-electron reduced forms.[60] This is understood to be a consequence of partitioning transferred charge over a larger and more electronically complex π-system which includes bidentate bonding to the metal center from the bipyridine itself. However, the motions observed, particularly in the case of **D3*** and **D3′*** where $\Delta\theta_1 = -30°$, are significant and certainly capable of tuning coupling between states having wave function character of adjacent π systems. Further, the torsional potential energy with respect to θ_1 is soft as determined for **D1***, particularly in the direction of decreasing θ_1 toward zero. With an enthalpic barrier height through $\theta_1 = 0°$ of only 0.4 kcal/mol (0.017 eV), real systems at room temperature are expected to sample a large distribution of θ_1 prior to ET events. Theory including dynamics with explicit solvation is warranted in the future.

The geometries of ET states support the reverse ligand based torsional switching hypothesized in the dynamic model presented in Scheme 1 where $\Delta\theta_1'$ (relative to the ^{3}D* dihedral angle) $= +6 \pm 3°, +8 \pm 3°, +18 \pm 3°, +23 \pm 8°$ for ^{3}**DA1**, ^{3}**DA2**, ^{3}**DA3**, and ^{3}**DA3′**, respectively (gas-phase calculations). That the magnitude of each of these is smaller than its forward counterpart $\Delta\theta_1$ mentioned above is understood in the context of Mulliken spin populations calculated from spin densities where it is seen that only 60−70% of transferred charge makes it to the acceptor while "pockets" remain on the asymmetric bipyridine proximal to the formal Ru^{III} center. These gas phase systems achieve a lower energy by allowing electron delocalization throughout the bpy-aryl-acceptor moiety, thereby, partially stabilizing the metal-centered hole at the expense of steric repulsions due to more coplanar geometries between aryl and bpy fragments.

The first confirmation of this idea comes from single point B3LYP calculations of these species embedded in an acetonitrile continuum model where ~ a full charge is observed via Mulliken spin populations on the acceptor. The second confirmation of this idea comes from a B3LYP geometry optimization of ^{3}**DA1** imbedded in an acetonitrile continuum. This system shows a spin population of ~ one on the acceptor and an energy relative to a continuum geometry optimization of the ground state singlet that is only 2% different than experiment (1.53 eV).[136] Most importantly from our point of view, $\Delta\theta_1' = +12°$ (relative to the B3LYP gas phase optimization of **D1***) to be compared with $\Delta\theta_1 = -13°$ (gas-phase B3LYP comparison between **D1*** and **DA1**) suggesting that with solvation the reverse torsional switching in these systems will go to completion. The implications of this result, especially in the context of the more sterically encumbered ^{3}**DA3** and ^{3}**DA3′**, are exciting.[149] In a simple model explored herein, where electronic coupling between

(149) While this manuscript was under review an optimization of ^{3}DA3′ within a PCM continuum model of acetonitrile converged. In this calculation $\theta_1 = 87.6°$, $\theta_2 = 1.4°$, and $CC_1 = 1.496$ Å. This value of θ_1 suggests a full reversal of the key torsional motion when a solvent model is included.

aryl and bipyridine fragments critical for superexchange in back ET varies as $\cos(\theta_1)$ or $\cos^2(\theta_1)$, the lifetime of charge separation in ^{3}**DA3** and ^{3}**DA3′** is predicted to be 139 or 19000 times larger, respectively, than that observed for ^{3}**DA1**. If forward ET can be kept efficient, and spin density predictions made in this paper suggest this is likely (especially for **DA3′**), such systems would be valuable molecular switches with a high quantum yield of charge separation and the capability of storing redox equivalents at moderate distances for a chemically significant amount of time.

Acknowledgment. We thank Professor Thomas Gray of Case Western Reserve University, Professor Robert Damrauer of the University of Colorado at Denver, and Dr. Jeffrey Hay and Dr. Roberto Bianco of the University of Colorado at Boulder for useful discussions. Professor Thomas Gray was also very helpful in optimizing a structure for comparative purposes. Dr. Nicole Eyet and Dr. Stephanie Villano helped with visualization software. Most of the computational resources were due to the National Science Foundation through their TeraGrid provided by the National Center for Supercomputing Applications. This material is based upon work supported by the University of Colorado and the National Science Foundation under Grant CHE-0847216. We also gratefully acknowledge support for in house computational infrastructure from the Chemical Sciences, Geosciences, and Biosciences Division, Office of Basic Energy Science, U.S. Department of Energy Grant DE-FG02-07ER15890.

Supporting Information Available: Additional information as noted in the text. This material is available free of charge via the Internet at http://pubs.acs.org.